CHALMERS
UNIVERSITY OF TECHNOLOGY

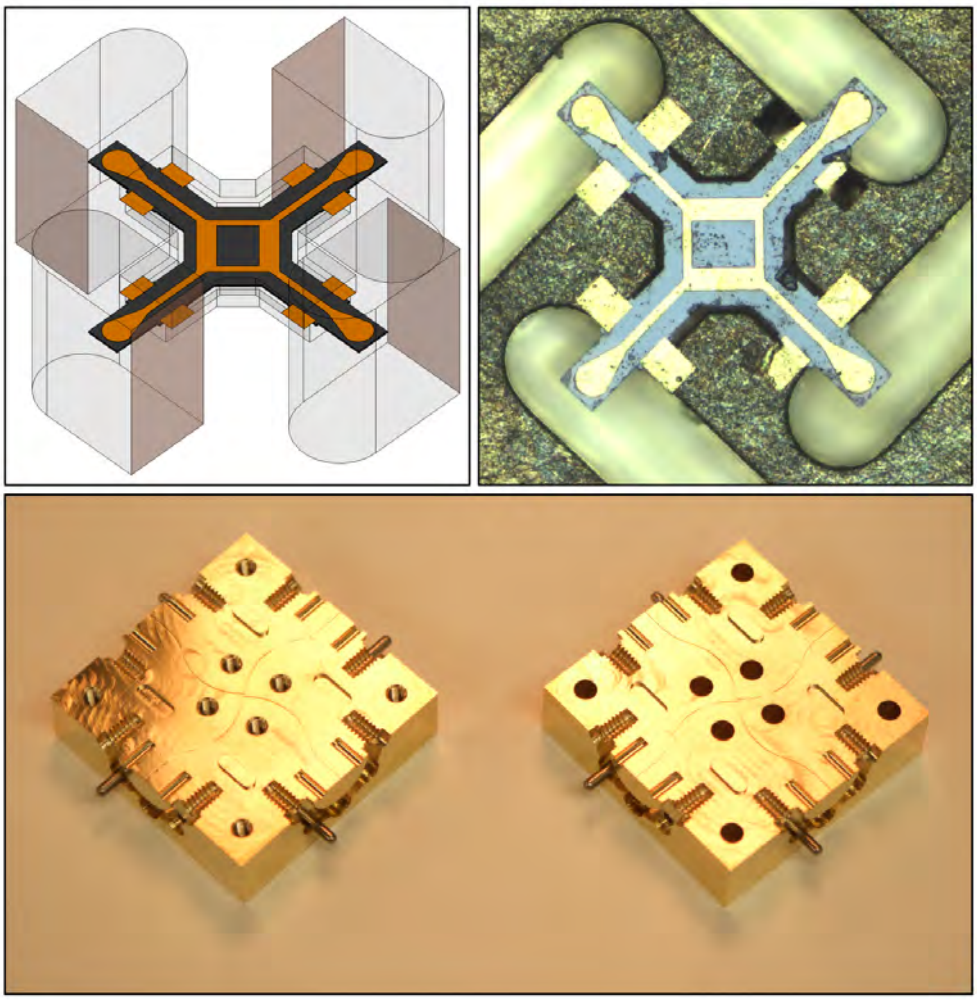

Design and characterisation of terahertz planar hybrids

Master's thesis in Wireless, Photonics and Space Engineering

ADITYA GOTURU

DEPARTMENT OF MICROTECHNOLOGY AND NANOSCIENCE
CHALMERS UNIVERSITY OF TECHNOLOGY
Gothenburg, Sweden 2025
www.chalmers.se

Master's thesis 2025

Design and characterisation of terahertz planar hybrids

ADITYA GOTURU

CHALMERS
UNIVERSITY OF TECHNOLOGY

Department of Microtechnology and Nanoscience
Terahertz and Millimetre Wave Laboratory
Chalmers University of Technology
Gothenburg, Sweden 2025

Design and characterisation of terahertz planar hybrids
ADITYA GOTURU 0000-0001-7269-0424

Supervisor and Examiner: Prof. Jan Stake, MC2

Master's Thesis 2025
Department of Microtechnology and Nanoscience
Terahertz and Millimetre Wave Laboratory
Chalmers University of Technology
SE-412 96 Gothenburg
Telephone +46 31 772 1000

Cover: A planar branch line coupler for a centre frequency of 925 GHz, in a WM-250 waveguide system, through the stages of design, fabrication and characterisation.

Typeset in LaTeX
Plots generated using OriginPro
Absolutely no Artificial Intelligence (AI) or Large Language Model (LLM) tools were used in any form to assist with the creation of this thesis.
Printed by Chalmers Reproservice
Gothenburg, Sweden 2025

Design and characterisation of terahertz planar hybrids
ADITYA GOTURU
Department of Microtechnology and Nanoscience
Chalmers University of Technology

Abstract

Power splitting and combining are essential functions in electronic and optical instruments. These functions are typically implemented using a directional coupler, which is a passive component found in various forms across the electromagnetic spectrum. These couplers are used to combine power sources, distribute signals for balanced and sideband-separating mixers, or redirect portions of signals for monitoring. At terahertz frequencies, the multi-section branch guide coupler, implemented in E-plane split block waveguide technology, is the most common version. However, the fabrication of these couplers is constrained by tight tolerances and high aspect ratio features, making them scale poorly at higher frequencies. There is a need to revisit this simple component and explore alternative implementations for integration with semiconductor devices that are rapidly being developed at terahertz frequencies.
In this work, three different planar hybrids operating in the 750 GHz to 1100 GHz frequency range are presented. Specifically, the branch-guide, broadside coupled line, and Lange couplers are evaluated through electromagnetic simulations. The 3-dB branch-guide coupler is fabricated and demonstrated on a 3-µm-thin silicon substrate using micro-fabrication and SOI technology. Gold beam leads are used to mechanically support the planar circuits in an E-plane split waveguide block.
The branch-guide coupler, after de-embedding from the 18 mm long access waveguides, showed a measured bandwidth of 17% over which the isolation was better than 15 dB, with over 40 dB of isolation at the centre frequency of 934 GHz. Over this band, the through and coupled signals remained over -4 dB, with amplitude balance better than 0.25 dB. The measurements agree well with simulations. The broadside coupled line and Lange coupler designs, from simulations, promise a flatter amplitude response across the band and improved phase balance. These results demonstrate the promising potential of planar couplers and hybrids at terahertz frequencies, for their use in more advanced receiver and transmitter circuits.

Keywords: directional couplers, hybrids, membrane circuits, sub-millimetre waves, terahertz technology

Acknowledgements

I would like to thank everyone at the Terahertz and Millimetre-wave Lab: Patrik, Nelson, Francesco, Shufei and Olivier for their support throughout this project. I would also like to thank Prof. Jeffrey Hesler, Dr. Josip Vukusic and Prof. Tomas Bryllert for their expertise and insight. Divya, thank you for introducing me to TML, and for all the proofreading. Malte and Jonathan, without your support and expertise, I would've had nothing to write a thesis about.

To all my friends, I am blessed to have you in my life: Michal, Hank, Tintin, Love, Rachel, Oskar, Xenia, Hanna, Agnes and everyone else at ETA, Kandu, Prateek, Murtuza, Raghavesh, Srikar, Nethra, Gitanjali, Raghav, Kartik, Husein and Achintya. Prof. KR Sarma, Dr. Bharghava Rajaram and Dr. Paromita Bose, without your guidance, I would not be here completing a Master's degree. Amma, Nanna and Anushka, I hope to see you in Europe next year.

I thank Prof. Helena Rodilla for the wonderful opportunity to work as an Amanuens at the Terahertz and Millimetre-wave Lab last year, and for pushing me through the exams.

Finally, I would like to thank Prof. Jan Stake, for many things, but, if nothing else, for sitting through my explanation of a Schottky barrier diode. I am excited for what the future holds, and, probably, the next round of semiconductor lectures.

This work, conducted within the Advanced Digitalization program at the WiTECH Centre CRYTER+, has been financed by VINNOVA, Chalmers University of Technology, Omnsisys Instruments AB (AAC Omnisys), Low Noise Factory (LNF), Research Institutes of Sweden (RISE) and Virginia Diodes Inc. (VDI).

Aditya Goturu, Gothenburg, July 2025

List of Acronyms

Below is the list of acronyms that have been used throughout this thesis listed in alphabetical order:

CAD	Computer Aided Design
CNC	Computer Numerical Control
DC	Direct Current
PEC	Perfect Electric Conductor
SoI	Silicon on Insulator
SOLT	Short, open, load, through
TE	Transverse Electric
TEM	Transverse Electro-magnetic
TM	Transverse Magnetic
VNA	Vector Network Analyzer

Nomenclature

Below is the nomenclature of parameters that have been used throughout this thesis.

Parameters

C	Coupling factor
Γ	Reflection coefficient
τ	Transmission coefficient
C	Coupling
D	Directivity
I	Isolation
L	Insertion Loss
v_p	phase velocity
v_{po}	phase velocity (odd mode)
v_{pe}	phase velocity (even mode)
Z_0	System impedance
Z_C	Characteristic impedance
Z_o	Odd mode impedance
Z_e	Even mode impedance
Z_{th}	Through line impedance
Z_{br}	Branch line impedance
Z_{IV}	Impedance (voltage and current definition)
Z_{PV}	Impedance (voltage and power definition)
Z_{PI}	Impedance (current and power definition)
Z_{EH}	Impedance (Wave definition)

Contents

List of Figures

List of Tables

1

Introduction

There is a need to combine or split power when designing instruments across the electromagnetic spectrum. In the domain of microwave systems, this need is fulfilled by power dividers [1] and directional couplers. At lower frequencies, there is a myriad [2] of implementations of directional couplers. In waveguide based systems, the large physical size of the waveguide allows for easy fabrication of electrically small features and complex topologies. The Bethe hole coupler [3] uses a rather thin waveguide wall, with a small hole, while the Magic-Tee hybrid [4] has waveguides extending outwards on all three axes. Couplers with larger features, such as the branch-guide coupler [5] and rat-race hybrid [6], are simpler to fabricate. These couplers can also be implemented in strip transmission line technologies such as stripline and micro-stripline, which provide more compact and tightly integrated systems, in the form of printed circuit boards and monolithic microwave integrated circuits. Such strip transmission lines support quasi-TEM propagation, which additionally allows the implementation of coupled line couplers [7] [8]. These couplers rely on the distributed capacitance acting between two strip transmission lines that are either next to, or on top of [9] each other. At terahertz and sub-terahertz frequencies, power dividers, instead of directional couplers, fulfil the requirements of many designs. They have often been implemented as Y-junctions in E-plane split-blocks [10], and even in planar technologies [11]. However, in many applications, such as the construction of sideband separating mixers for radio astronomy [12], or in atmospheric radar receivers [13], there is a strong need for terahertz directional couplers.

Miniscule size of features and high loss are some of the biggest challenges to implementing microwave circuits at terahertz frequencies. The vast majority of terahertz directional couplers are based on multi-section branch-guide designs. Designs for these couplers were first tabulated by Reed [14], and Levy et al. [15]. However even a cursory glance at these tables reveals a problem - low impedance branch waveguides require very high aspect ratio slots to be fabricated, connecting the two main waveguides. The most straightforward way to implement these branch-guide couplers is CNC micro-milling [16]. Modern micro-milling is limited to tool aspect ratios of 1:3 [17], rendering most of the tabulated designs impossible to fabricate. Many contemporary designs, for instance the hybrid used by Khudchenko et al. [18] to drive an SIS mixer, use computational optimization to find best-fit designs for branch-guides while limiting the geometry to what can be fabricated. The height of

the parent waveguide has been altered by Sobis et al. [19] and Rashid et al. [20] to slightly improve the achievable impedance ratios, however, this technique is limited by the propagation of higher order modes. A group from JPL has demonstrated micro-fabrication techniques [21] to pattern the waveguide structures onto silicon. Similar techniques were used to implement a hybrid at 230-300 GHz by a group from The Royal Institute of Technology (KTH), Sweden [22]. At Chalmers, the metal E-plane split blocks have even been grown on a lithographically patterned mould [23]. While using such techniques to produce waveguide blocks is feasible, there is another limitation as these designs are scaled to higher frequencies: the alignment of the two split-plane halves with each other. Even a small misalignment can completely displace the narrow finger structures. There remains a need to explore alternate technologies for implementing directional couplers and hybrids that is easier to scale into higher frequencies, to replace the waveguide split-plane multi-section branch-guide coupler.

In 2006, Vassilev et al. [24] presented multi-section couplers at 300 GHz using lithographically produced E-field probes connected by microstrip lines, acting as the branches. However, this technique was reported to be difficult to fabricate even at low frequencies, and ultimately relies on a great deal of mechanical precision while assembling. In 2020, this work was extended [25] to alleviate the alignment concerns by incorporating all branches into a single chip, however, the challenges still remain when trying to reach higher coupling factors. In 2010, a fully planar implementation of a directional coupler was presented by Virginia Diodes (VDI) [26], where coplanar coupled lines are implemented in shielded microstrip, produced using a combination of CNC micro-milling for the channel and lithographic micro-fabrication for the substrate and centre conductors. A coupling factor of -7 dB was achieved, which does not allow for the implementation of a symmetric hybrid, with an equal power split and a 90° phase difference between outputs.

This work presents three designs of terahertz planar hybrids, for the WM-250 [27] waveguide band. These hybrid couplers are realized in shielded suspended stripline technology, with a CNC micro-milled channel supporting a SOI membrane on gold beam-leads. The first is a simple branch-guide coupler. The next is a modified broadside coupled line, which accounts [28] for the high dielectric constant of the substrate [29]. The final design is based on a Lange coupler [30], with a similar effect caused by the high dielectric constant.

The outline of this thesis is as follows. Chapter 2 covers the theoretical background necessary to understanding the coupler designs, such as the circuit theory analysis techniques and an overview of different waveguide structures. Chapter 3 presents the methods used in the simulation, fabrication and characterization of these couplers. Chapter 4 presents the results of these simulations and measurements. Out of the three designs, the branch-line coupler was chosen as a candidate for fabrication. Its design was further optimized, a tolerance analysis was performed and it was fabricated in-house by CNC micro-milling and lithographic micro-fabrication. Chapter 4 additionally presents preliminary results from these simulations, however, at the time of writing, more comprehensive measurements are still underway, and results will follow in a future publication.

2

Theory

In this chapter, the theory and background behind the design of terahertz directional couplers is examined. Various topologies are described and the considerations behind choices made in this work are explained.

2.1 Directional couplers and hybrids

Couplers are passive devices that split, or couple, a portion of incident power at one port to another port. It can be shown [31] that a three-port network cannot simultaneously be lossless, reciprocal, and matched at all ports. Power dividers [1] and combiners are examples of such three-port networks. Four-port networks can be lossless, reciprocal and matched on all ports at the same time. It is possible to terminate one port to turn a four-port network into a three-port, however, the network then becomes lossy, as power delivered to the matched termination is lost.

A directional coupler [2] is a lossless, reciprocal, four-port network, matched on all ports, that delivers power incident on a port to a corresponding transmission or "through" port, while redirecting a fixed proportion of that power to a coupled port. No power is delivered to the fourth port, called the isolated port. However, when power is incident on the through port, the coupled power is delivered to this fourth port instead, making the coupled port "directional", hence the name.

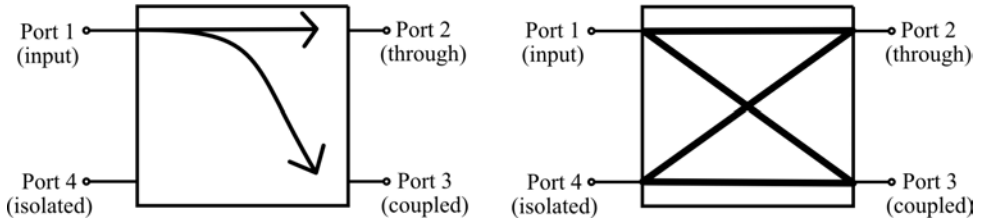

Figure 2.1: Symbols for a directional coupler (left) and hybrid (right). The port layout or numbering does not represent the physical layout, and different physical topologies will result in different ports being through, coupled or isolated.

When discussing couplers, the following parameters are often used as figures of merit (referenced to power incident on port 1, however, due to reciprocity, these can be rewritten for all ports):

$$\text{Coupling} = C = 10\log(\frac{P1}{P3}) = -20\log(|S_{31}|) \text{ dB} \tag{2.1a}$$

$$\text{Directivity} = D = 10\log(\frac{P3}{P4}) = -20\log(\frac{|S_{31}|}{|S_{41}|}) \text{ dB} \tag{2.1b}$$

$$\text{Isolation} = I = 10\log(\frac{P1}{P4}) = -20\log(|S_{41}|) \text{ dB} \tag{2.1c}$$

$$\text{Return loss} = R = -20\log(|S_{11}|) \text{ dB} \tag{2.1d}$$

The above figures of merit are all positive quantities, and are primarily used in textual descriptions of couplers. However, when presenting data graphically, it is common convention to plot the magnitude of the underlying S-parameters directly. This is simply a change of sign.

Amplitude balance is the ratio of power delivered to the through port and the coupled port, while phase balance is the phase difference between the through and coupled ports (typically quadrature or anti-phase).

A hybrid coupler, or just hybrid, is a special case of a directional coupler, designed to split the incident power equally between the through and coupled ports. They are sometimes called 3 dB couplers, referring to the coupling C.

2.2 Ideal couplers

The S-matrix of a reciprocal coupler that is matched at all ports is given by:

$$[\mathbf{S}] = \begin{bmatrix} 0 & S_{21} & S_{31} & 0 \\ S_{21} & 0 & 0 & S_{31} \\ S_{31} & 0 & 0 & S_{21} \\ 0 & S_{31} & S_{21} & 0 \end{bmatrix} \tag{2.2}$$

Where S_{21} is the transmission factor, and S_{31} is the coupling factor. In order for the network to be lossless, it can be shown [31] that there exist two valid solutions for the phase difference between the outputs. The first is the symmetric case:

$$[\mathbf{S}] = \begin{bmatrix} 0 & \sqrt{1-C^2} & jC & 0 \\ \sqrt{1-C^2} & 0 & 0 & jC \\ jC & 0 & 0 & \sqrt{1-C^2} \\ 0 & jC & \sqrt{1-C^2} & 0 \end{bmatrix} \tag{2.3}$$

The second is the anti-symmetric case:

$$[\mathbf{S}] = \begin{bmatrix} 0 & \sqrt{1-C^2} & C & 0 \\ \sqrt{1-C^2} & 0 & 0 & -C \\ C & 0 & 0 & \sqrt{1-C^2} \\ 0 & -C & \sqrt{1-C^2} & 0 \end{bmatrix} \tag{2.4}$$

In both cases, C is the coupling factor. If the coupling and transmission factors are equal, $C = 1/\sqrt{2}$, and the S matrix of the resulting symmetric hybrid coupler is given by:

$$[\mathbf{S}] = \frac{1}{\sqrt{2}} \begin{bmatrix} 0 & 1 & j & 0 \\ 1 & 0 & 0 & j \\ j & 0 & 0 & 1 \\ 0 & j & 1 & 0 \end{bmatrix} \tag{2.5}$$

This thesis focuses only on symmetric hybrid couplers. These are also called quadrature hybrids, as two signals 90° apart are said to be in quadrature.

2.2.1 Branch-guide coupler

The ideal circuit for a branch-guide coupler, shown in Figure 2.2, was described by Young in [32]. In the paper, the behaviour of the coupler was analysed using the odd/even analysis method [33], summarized below.

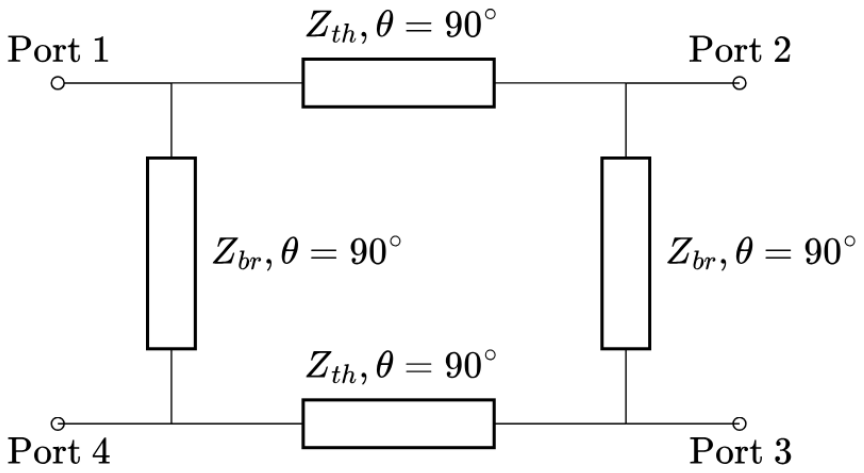

Figure 2.2: A branch-guide coupler.

It is assumed that all ports are terminated with impedance Z_0. The circuit is excited with two pairs of voltages on ports 1 and 4: V^+, V^+ for the even case and V^+, $-V^+$ for the odd case.

For the even case, even excitation implies that no current flows through the line of symmetry, i.e it is an open circuit at $\theta = 45°$. The circuit can then be analysed as a two port network. In the odd case, the voltage at the plane of symmetry is 0 V, therefore it is a short-circuit.

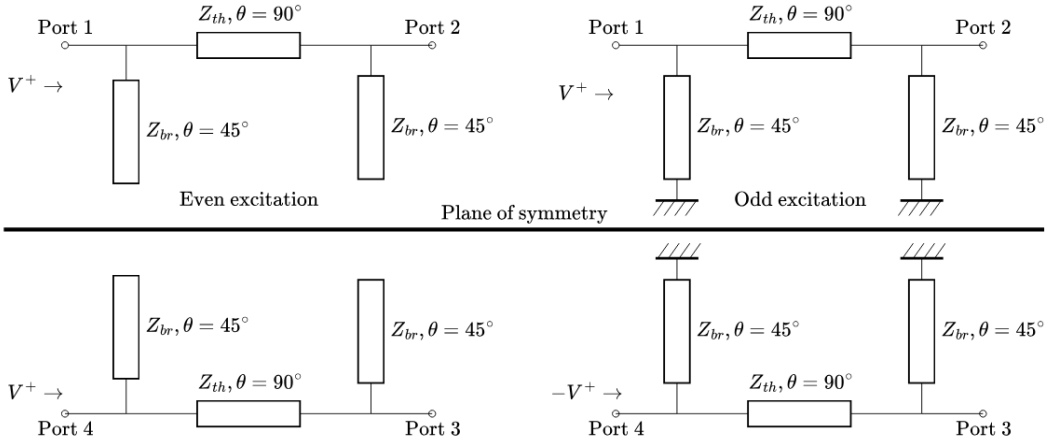

Figure 2.3: Even and odd excitations of the branch-guide coupler circuit.

From the vertical symmetry, the scattering matrix can be found for the odd and even cases:

$$\left[\mathbf{S_e}\right] = \begin{bmatrix} \Gamma_e & T_e \\ T_e & \Gamma_e \end{bmatrix} \tag{2.6a}$$

$$\left[\mathbf{S_o}\right] = \begin{bmatrix} \Gamma_o & T_o \\ T_o & \Gamma_o \end{bmatrix} \tag{2.6b}$$

ABCD matrix for cascaded circuits can be found by multiplying them. The ABCD matrix for the stubs and the line is known [34], and therefore the ABCD for the even mode circuit is given by:

$$\begin{bmatrix} A & B \\ C & D \end{bmatrix}_e = \begin{bmatrix} A & B \\ C & D \end{bmatrix}_{stub} \begin{bmatrix} A & B \\ C & D \end{bmatrix}_{line} \begin{bmatrix} A & B \\ C & D \end{bmatrix}_{stub} \tag{2.6c}$$

$$\begin{bmatrix} A & B \\ C & D \end{bmatrix}_e = \begin{bmatrix} 1 & 0 \\ jY_{br} & 1 \end{bmatrix} \begin{bmatrix} 0 & jZ_{th} \\ jZ_{th} & 0 \end{bmatrix} \begin{bmatrix} 1 & 0 \\ jY_{br} & 1 \end{bmatrix} \tag{2.6d}$$

$$\begin{bmatrix} A & B \\ C & D \end{bmatrix}_e = \begin{bmatrix} -Y_{br}Z_{th} & jZ_{th} \\ j(Y_{th} - Y_{br}^2 Z_{th}) & -Y_{br}Z_{th} \end{bmatrix} \tag{2.6e}$$

Similarly, for the odd-mode, the short circuit at the symmetry plane results in the ABCD matrix being:

$$\begin{bmatrix} A & B \\ C & D \end{bmatrix}_o = \begin{bmatrix} Y_{br}Z_{th} & jZ_{th} \\ j(Y_{th} - Y_{br}^2 Z_{th}) & Y_{br}Z_{th} \end{bmatrix} \tag{2.6f}$$

Converting the ABCD matrix back to S-parameters [35] gives:

$$\Gamma_e = \frac{Z_{th}^2 Y_0^2 - Z_0^2(Y_{th} - Y_{br}^2 Z_{th})^2 - j(2Y_{br}Z_{th}(Z_{th}Y_0 - Y_{th}Z_0 + Y_{br}^2 Z_{th}Z_0))}{4Y_{br}^2 Z_{th}^2 + (Z_{th}Y_0 + Y_{th}Z_0 - Y_{br}^2 Z_{th}Z_0)^2} \tag{2.6g}$$

$$T_e = \frac{-4Y_{br}^2 Z_{th} - 2j(Z_{th}Y_0 + Y_{th}Z_0 - Y_{br}^2 Z_{th}Z_0)}{4Y_{br}^2 Z_{th}^2 + (Z_{th}Y_0 + Y_{th}Z_0 - Y_{br}^2 Z_{th}Z_0)^2} \tag{2.6h}$$

$$\Gamma_o = \frac{Z_{th}^2 Y_0^2 - Z_0^2(Y_{th} - Y_{br}^2 Z_{th})^2 + 2jY_{br}Z_{th}(Z_{th}Y_0 - Y_{th}Z_0 + Y_{br}^2 Z_{th}Z_0)}{4Y_{br}^2 Z_{th}^2 + (Z_{th}Y_0 + Y_{th}Z_0 - Y_{br}^2 Z_{th}Z_0)^2} \tag{2.6i}$$

$$T_o = \frac{4Y_{br}^2 Z_{th} - 2j(Z_{th}Y_0 + Y_{th}Z_0 - Y_{br}^2 Z_{th}Z_0)}{4Y_{br}^2 Z_{th}^2 + (Z_{th}Y_0 + Y_{th}Z_0 - Y_{br}^2 Z_{th}Z_0)^2} \tag{2.6j}$$

The definition of the S-matrix is:

$$\begin{bmatrix} V_1^- \\ V_2^- \\ V_2^- \\ V_2^- \end{bmatrix} = [\mathbf{S}] \begin{bmatrix} V_1^+ \\ V_2^+ \\ V_2^+ \\ V_2^+ \end{bmatrix} \tag{2.6k}$$

The excitations used for the even and odd case are:

$$\begin{bmatrix} V^+ \\ 0 \\ 0 \\ V^+ \end{bmatrix} \text{ and } \begin{bmatrix} V^+ \\ 0 \\ 0 \\ -V^+ \end{bmatrix} \tag{2.6l}$$

Therefore, the excitations can be added to produce:

$$\begin{bmatrix} V^+ \\ 0 \\ 0 \\ V^+ \end{bmatrix} + \begin{bmatrix} V^+ \\ 0 \\ 0 \\ -V^+ \end{bmatrix} = \begin{bmatrix} 2V^+ \\ 0 \\ 0 \\ 0 \end{bmatrix} \tag{2.6m}$$

$$\gamma_{11} = \frac{\Gamma_e + \Gamma_o}{2} \tag{2.6n}$$

Similarly, by adding or subtracting the excitations, the transmission to all three other ports can be calculated:

$$\alpha_{12} = \frac{T_e + T_o}{2} \tag{2.6o}$$

$$\beta_{13} = \frac{T_e - T_o}{2} \tag{2.6p}$$

$$\delta_{14} = \frac{\Gamma_e - \Gamma_o}{2} \tag{2.6q}$$

Then, symmetry can be used to fill in the entire S-matrix, giving:

$$S = \begin{bmatrix} \gamma_{11} & \alpha_{12} & \beta_{13} & \delta_{14} \\ \alpha_{12} & \gamma_{11} & \delta_{14} & \beta_{13} \\ \beta_{13} & \delta_{14} & \gamma_{11} & \alpha_{12} \\ \delta_{14} & \beta_{13} & \alpha_{12} & \gamma_{11} \end{bmatrix} \quad \text{with} \quad \alpha^2 + \beta^2 = 1 \tag{2.6r}$$

While the derivation has been omitted from this text, it is possible to show that for the following branch and through impedances, asserting that all ports are matched and perfect isolation:

$$\gamma_{11} = 0 \tag{2.6s}$$

$$\delta_{14} = 0 \tag{2.6t}$$

$$Z_{br} = Z_0 \tag{2.6u}$$

$$Z_{th} = \sqrt{2}Z_0 \tag{2.6v}$$

The S-matrix simplifies to:

$$\alpha_{12} = \frac{1}{\sqrt{2}} \tag{2.6w}$$

$$\beta_{13} = j\alpha_{12} = \frac{j}{\sqrt{2}} \tag{2.6x}$$

This is the case for a branch-guide hybrid. The final S-matrix of this hybrid is now:

$$[\mathbf{S}] = \frac{1}{\sqrt{2}} \begin{bmatrix} 0 & 1 & j & 0 \\ 1 & 0 & 0 & j \\ j & 0 & 0 & 1 \\ 0 & j & 1 & 0 \end{bmatrix} \tag{2.6y}$$

This is the same as Equation 2.5.

2.2.2 Coupled line coupler

Coupled line couplers, as described by Jones in [8], can also be analysed using the above odd/even method.

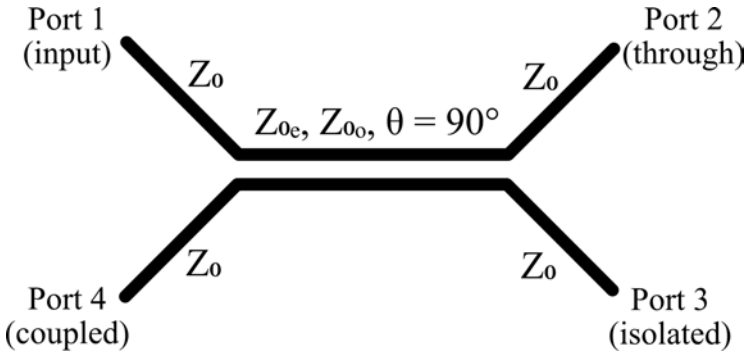

Figure 2.4: A coupled line directional coupler.

A coupled line coupler is coupled transmission line that is a quarter-wavelength (90°) long at it's centre frequency, and each of the conductors are driven by a source impedance Z_0 such that:

$$Z_0 = \sqrt{Z_e Z_o} \tag{2.7a}$$

The coupling factor can be set to C by choosing odd and even mode impedances such that:

$$Z_o = Z_0 \sqrt{\frac{1-C}{1+C}} \tag{2.8a}$$

$$Z_e = \frac{Z_0^2}{Z_o} \tag{2.8b}$$

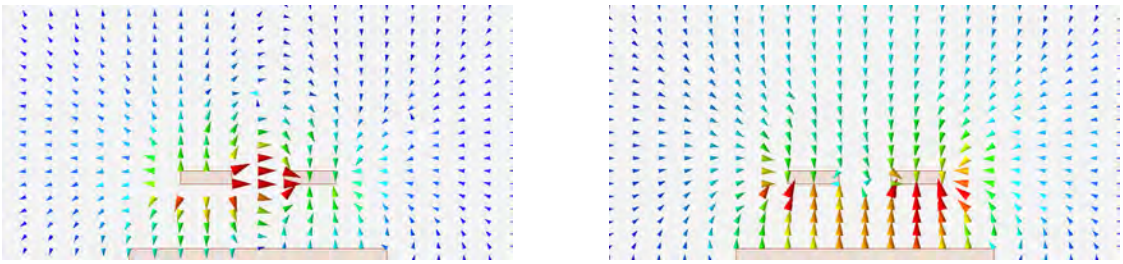

Figure 2.5: Odd (left) and even (right) excitations in a three-conductor waveguide.

For a coupling factor of $1/\sqrt{2}$ (equal power split), the ratio $Z_e : Z_o$ is approximately equal to 6.

2.2.3 Multi-section couplers

There are many techniques for improving the usable bandwidth of hybrids. In the case of branch-guide couplers, these techniques are based on increasing the number of branches to engineer a desired frequency response [14]. These designs always require high aspect ratio branches for the outermost lines. For coupled lines, multiple, increasingly coupled quarter-wave sections are symmetrically cascaded to improve bandwidth.

This thesis focuses on the technology in which couplers are implemented. As such, the multi-section coupler designs are beyond the scope of this thesis and will not be discussed in further detail.

2.3 Waveguides

Waveguides are structures that confine and guide an electromagnetic wave with minimal loss over an indefinite length. They often have a constant cross-section in the plane of propagation. When the size of this cross-section is negligible compared to the wavelength in the medium, waveguides can be seen as transmission lines.

2.3.1 Modes

Fields in waveguides propagate in discrete modes: field patterns that represent an eigensolution of Maxwell's equations over the cross-section. If a solution has no E-field or H-field component in the direction of propagation, it is known as a transverse electro-magnetic (TEM) mode. If a mode has a small E-field or H-field component, but the pattern otherwise resembles a TEM mode, it is called a quasi-TEM mode. These are typically seen in waveguides with two or more conductors. TEM and quasi-TEM modes can propagate at all frequencies.

If the field solutions have a significant E-field or H-field component, they are known as transverse magnetic (TM) or transverse electric (TE) modes, respectively. These modes are seen in all waveguides, even those with only one conductor. They are heavily attenuated below a certain frequency, f_c, known as the mode's cut-off frequency.

Two modes with the same f_c are known as degenerate modes. The propagation constant for each mode can be derived from the field solution. If two degenerate modes have the same propagation constant, then it is possible to view the resulting field pattern as a superposition of the constituent modes. These are known as hybrid modes, and they can have significant E-field and H-field components in the direction of propagation. In waveguides with three or more conductors, two or more degenerate TEM or quasi-TEM modes may propagate.

When a waveguide is excited with a frequency that is beyond the f_c for multiple modes with different propagation constants, power is split between these modes. This may be undesirable as it causes dispersion. Thus, waveguides are typically

designed to be operated below the f_c for unwanted higher-order modes, known as parasitic modes. The mode with the lowest f_c is called the principal or fundamental mode. In multi-conductor waveguides, the TEM or quasi-TEM modes, propagating from DC, are the fundamental modes.

2.3.2 Propagation parameters

A waveguide generally has a well-defined β (and thus v_p) for each mode, which relates phase across a length of waveguide. This allows the waveguide to be modelled as a transmission line. It is often possible to define the characteristic impedance, Z_C of waveguides, especially in the case of the fundamental mode of multi-conductor waveguides [36].

In a circuit model, such discontinuities may be seen as additional inductances and capacitances at the junction. Since the advent of easily accessible computational electromagnetic simulation software, which directly solve Maxwell's equations in three dimensions, it is more common that engineers will simply find the circuit port parameters of the whole junction rather than modelling it with components.

2.3.3 Transmission lines

Transmission lines are a useful component for modelling the behaviour of various types of waveguides.

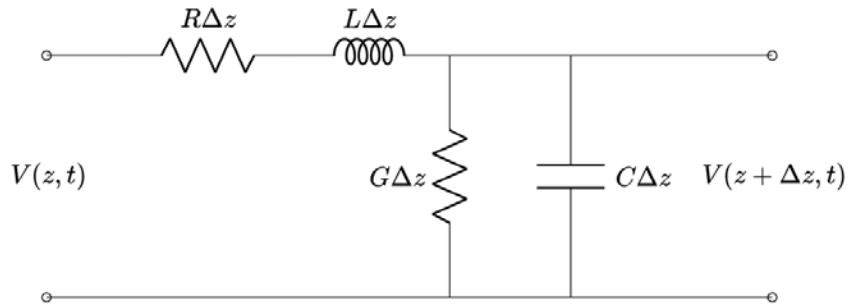

Figure 2.6: A circuit representation of a section of a transmission line.

Transmission lines are represented by pairs of conductors, and defined by a characteristic impedance:

$$Z_C = \sqrt{\frac{L}{C}} \tag{2.9}$$

Where L and C are the distributed inductance and capacitance over some length of the line. It is also useful to define the propagation constant and phase velocity:

$$\beta = \frac{2\pi}{\lambda} \tag{2.10a}$$

$$v_p = \frac{1}{\sqrt{\epsilon\mu}} = \frac{\omega}{\beta} \tag{2.10b}$$

Where λ is the guided wavelength of the signal. For a general transmission line, the propagation constant can be complex, represented as:

$$\gamma = \alpha + j\beta \tag{2.11}$$

Where α represents the loss. For a lossless (ideal) transmission line, this is 0, and:

$$\gamma = j\beta \tag{2.12a}$$

$$\beta = \omega\sqrt{LC} \tag{2.12b}$$

When a transmission line of length ℓ and characteristic impedance Z_C is terminated with a load impedance Z_L, the impedance seen at the beginning of the transmission line, Z_{in}, can be expressed as:

$$Z_{\text{in}} = Z_C \frac{Z_L + jZ_C \tan(\theta)}{Z_C + jZ_L \tan(\theta)} \tag{2.13a}$$

where:

$$\theta = \beta\ell \tag{2.13b}$$

The electrical length, θ, is assumed to be linearly dependent on frequency for ideal transmission lines. In practice, real waveguides modelled by transmission lines may have a non-linear relationship between frequency and β, and thus θ and v_p. This is known as dispersion.

2.3.4 Rectangular waveguides

A rectangular waveguide is a hollow rectangular tube. A standard rectangular waveguide has an aspect ratio of 1:2. The field patterns for the first few modes are shown in Figure 2.7. These modes are classified as either TE or TM modes, as all solutions have either an E-field or H-field component that is non-zero in the direction of propagation. The fundamental mode, called TE_{10}, can be operated until

the next mode, TE_{01} starts to propagate. Typically, a rectangular waveguide has about 30% usable bandwidth.

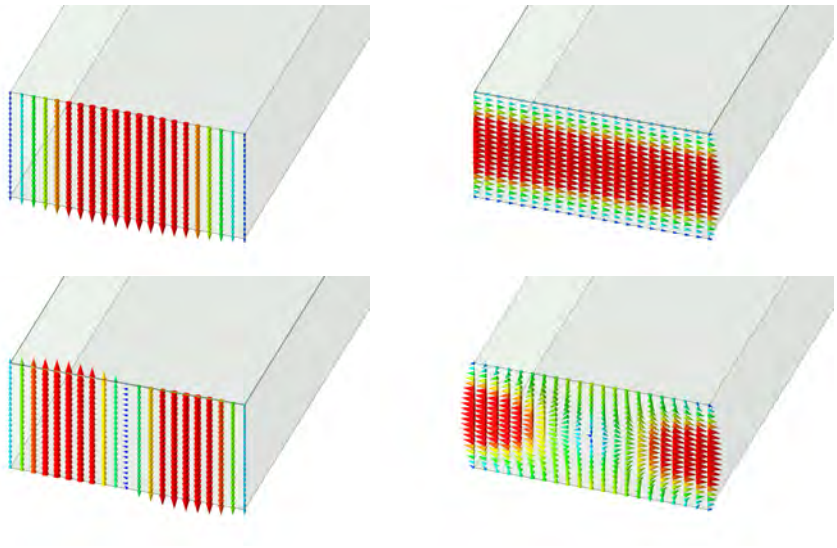

Figure 2.7: The fundamental mode (TE_{10}) and higher order modes (TE_{01}, TE_{20} and TM_{11}) in a rectangular waveguide.

While β is dispersive, it can often be approximated as linear, near the centre or high-end of the band. It is well-defined for a mode, and can be found from the field solution. The wave impedance, Z_{EH}, is defined as the ratio of the transverse E-field and H-field components. This definition is adequate for applying circuit theory to TEM based waveguides, but not for TE or TM modes. For the TE_{10} mode, from pairs of power, voltage and current, a characteristic impedance can be defined as [37]:

$$Z_{PI} = Z_{EH} \times \pi^2 b/8a \tag{2.14a}$$

$$Z_{VI} = Z_{EH} \times \pi b/2a \tag{2.14b}$$

$$Z_{PI} = Z_{EH} \times 2b/a \tag{2.14c}$$

Where a and b are the broad and narrow-wall dimensions of the rectangular waveguide.

These definitions are useful when modelling different types of waveguide junctions with transmission line models. For example, when studying a T-junction of three waveguides with different heights, the definition Z_{EH} is not appropriate, and one of the above definitions must be used. On the other hand, a step change in the dielectric would be adequately modelled by Z_{EH}.

The plane perpendicular to broad-wall is known as the E-plane, while the plane perpendicular to the narrow-wall is called the H-plane. No currents flow through the E-plane at the centre of a waveguide, and therefore, when fabricating a waveguide,

it is preferred to split the conductor along this plane, to minimize the impact of imperfections on the waveguide.

2.3.5 Coaxial lines

A coaxial line is a waveguide consisting of two conductors - a centre wire, and a shield surrounding it. It's fundamental mode and first higher-order mode is shown in Figure 2.8. The fundamental mode propagates from DC, while higher-order modes have a cutoff frequency defined by the dimensions of the outer shield and the dielectric. The fundamental mode has no E-field or H-field components in the direction of propagation, thus it is a TEM mode.

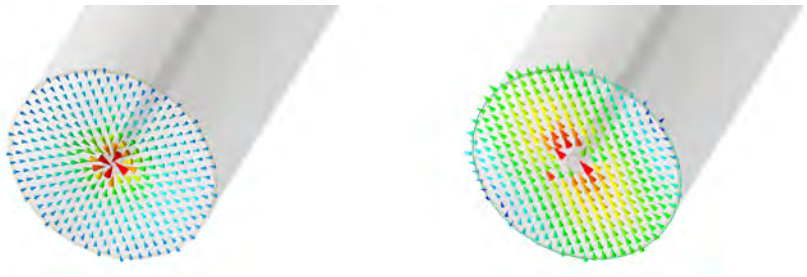

Figure 2.8: The dominant TEM mode and a parasitic TE_{11} mode in a coaxial line.

2.3.6 Planar (strip) waveguides

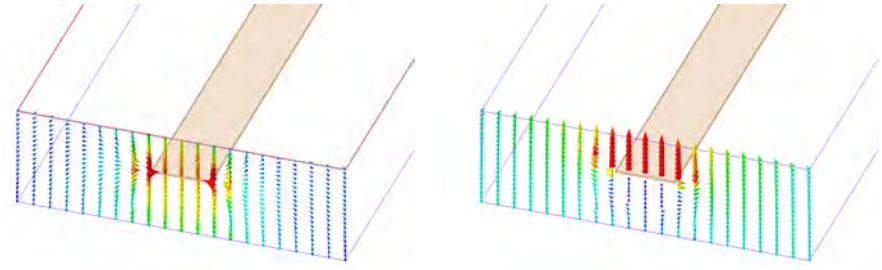

Figure 2.9: The fundamental TEM mode and a higher order parasitic mode in a shielded stripline

Striplines, micro-striplines, shielded striplines and shielded microstrips are all examples of planar waveguides, called so due to the flat strip-line nature of their signal conductor. Due to their structure, it is possible to have multiple signal conductors in such a waveguide, and when close enough, the fields will strongly interact.

The field solutions for the fundamental modes and higher order modes of a shielded stripline are shown in Figure 2.9. These fundamental modes all behave like TEM modes, however, due to asymmetry, they may have a small field component in the direction of propagation, and are thus called quasi-TEM modes.

In the case of three or more conductors, it is convenient to define the even and odd mode impedances, Z_e and Z_o.

3

Methods

In this chapter, the methods used for the design, simulation, fabrication and characterisation of planar terahertz hybrids are discussed.

3.1 Design

3.1.1 Shielded and suspended striplines

The planar hybrids were designed to operate in the WM-250 [27] band, from 750 to 1100 GHz, with a centre frequency around 925 GHz. This allows S-parameter characterisation and verification using a Vector Network Analyser (VNA).

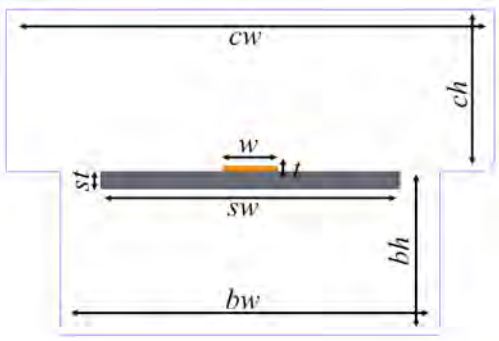

Figure 3.1: The cross section of the shielded suspended stripline channel. Dimensions are provided in Table 3.1

The planar circuits were designed as shielded suspended striplines, which can be mounted in an E-plane split block using beam-lead technology. Hence, a transition from the stripline's fundamental mode to the WM-250 waveguide's TE_{10} mode is required. A shielded suspended stripline cross section, to be used as the feed lines for the hybrid was first designed and simulated. A 3-μm silicon membrane was chosen as the substrate. Figure 3.1 shows the designed channel, with dimensions tabulated below in Table 3.1. It is assembled from two blocks, which mate along the center-line. The split is coplanar with the centre E-plane of the waveguide. The top half of the channel is designed to be larger, to accommodate misalignment of the two halves.

Table 3.1: Design parameters of the suspended stripline channel.

Parameter	Value
cw	90 μm
ch	30 μm
bw	70 μm
bh	30 μm
sw	55 μm
st	3 μm
w	10 μm
t	0.3 μm

2D port-only solutions of this cross section were calculated using an electromagnetic solver (see 3.2). The impedance was found to be $Z_0 = 120\ \Omega$ at 925 GHz. At 925 GHz, a quarter-wavelength section is about 75μm long. The first higher-order mode was found to begin propagating, albeit with strong attenuation, at around 1.75 THz. This leaves some overhead for the channel to be widened to accommodate the hybrid without exciting higher order modes.

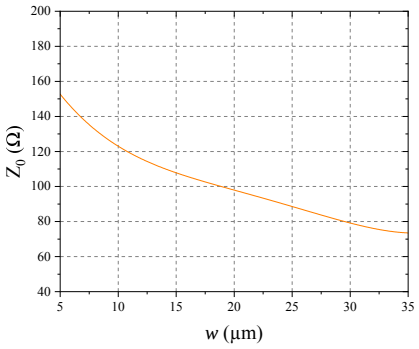

Figure 3.2: Impedance of stripline channel as a function of conductor width.

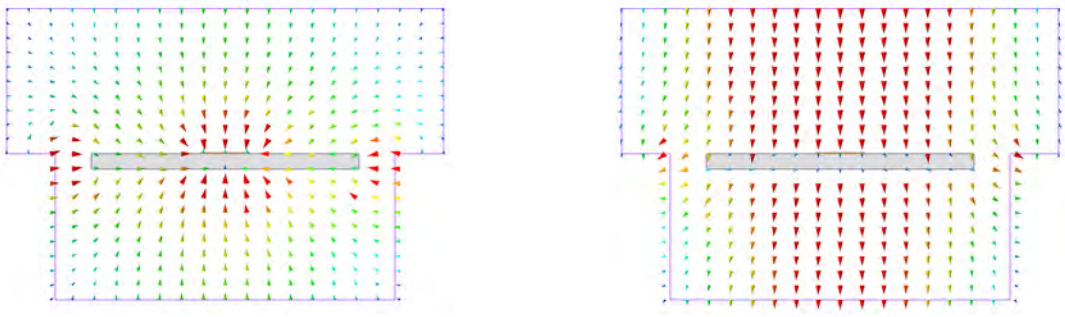

Figure 3.3: The fundamental quasi-TEM mode (left) and first higher-order mode (right) in the waveguide channel.

3.1.2 Transition

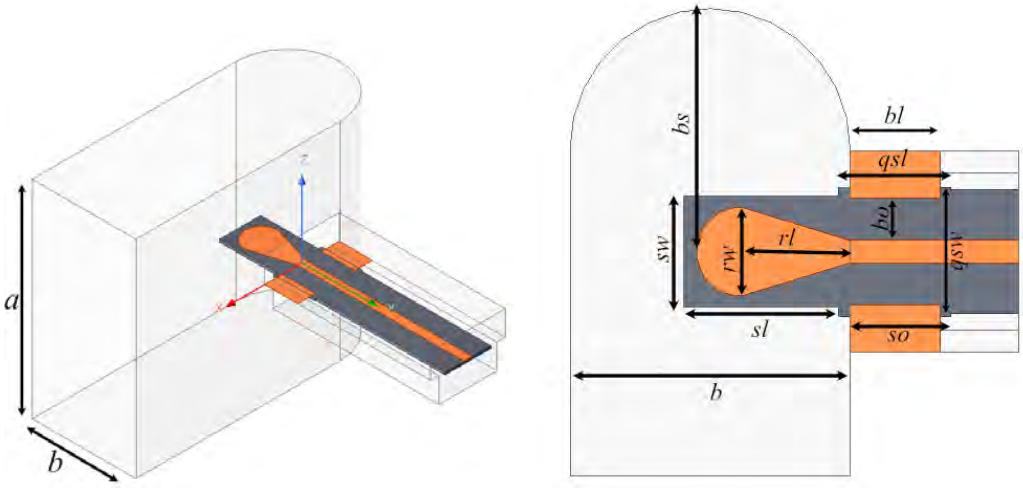

Figure 3.4: The transition from WM-250 waveguide to the suspended stripline channel. Dimensions provided in Table 3.2.

A waveguide transition, between the WM-250 waveguide's TE_{10} mode and the stripline's fundamental quasi-TEM mode, was designed in the style of a radial probe, as described in [38]. Mechanical beam-leads were integrated into the probe design, allowing the hybrid to be designed without having to consider the beam-lead coupling. The final design was produced by using the optimisation tool in the electromagnetic solver, which automatically adjusted the dimensions until the desired return loss was achieved.

Table 3.2: Design parameters of the WM-250 waveguide to suspended stripline transition.

Parameter	Value
sw	49.5 μm
sl	69.5 μm
rw	39.5 μm
rl	48.5 μm
bs	108 μm
qsw	57.5 μm
qsl	50 μm
so	45 μm
bl	40 μm
bo	18.9 μm
a	250 μm
b	125 μm

3.1.3 Design flow and optimisation

For each hybrid, the first step was to use a linear circuit simulator to create a model based on ideal transmission lines. This was done to validate the design and study the impact of deviating electrical lengths and impedances.

Next, the necessary line components were physically realised. Impedances and propagation factors for each required line were calculated using the 2D port-solver feature of our electromagnetic simulator.

Finally, an ideal 3D model was created with those line components in an electromagnetic simulator, and the behaviour of this model was compared to the ideal circuit. Deviating properties were identified and the relevant dimensions of the 3D model were altered to correct it. This process was iterated, while making the model more realistic, and eventually adding the waveguide transitions. Finally, a tolerance analysis was performed, to study the impact of various misalignments during fabrication.

3.1.4 Branch-guide coupler

The branch-guide hybrid coupler described by Young [32] was implemented as shown in Figure 3.5. The branch-guide has the same impedance as the feed line ($Z_{br} = Z_0 = 120\ \Omega$), and the through-line has an impedance $Z_{th} = Z_0/\sqrt{2}\ \Omega \approx 85\Omega$, which was found to correspond to a conductor width of 23 μm (see Figure 3.4). However, as the through and branch-guides have a different effective channel width due to the structure, after tuning, this value was found to be closer to 24 μm. For a detailed drawing of the final membrane with transitions, see Appendix B.

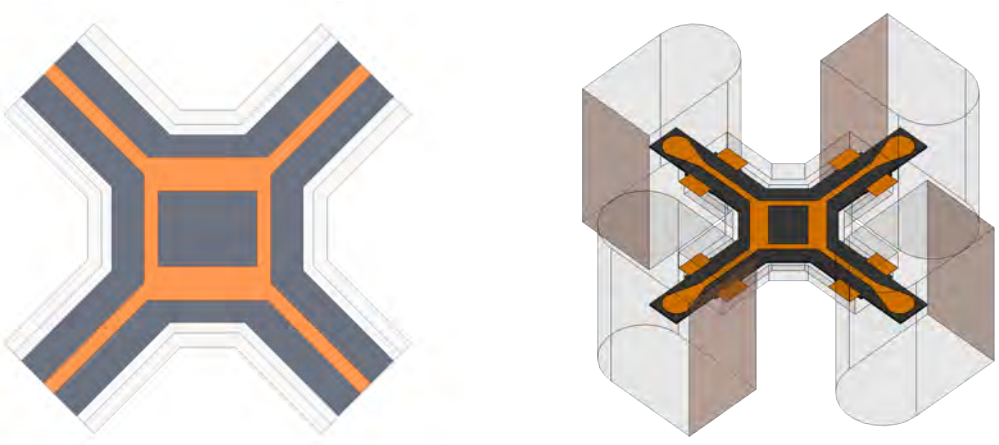

Figure 3.5: Branch-guide coupler in shielded suspended stripline (left), and embedded in four waveguide to stripline transitions (right).

3.1.5 Inhomogeneous broadside coupled line coupler

From the equations presented by Dalley [28], it can be calculated that to achieve a -3 dB coupling factor, the ratio of the even and odd mode impedances ($Z_o : Z_e$) must be approximately 6, and the ratio of their phase velocities ($v_{po} : v_{pe}$) must be 3.

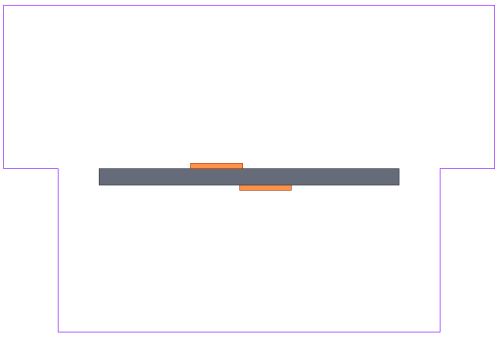

Figure 3.6: Coupled stripline cross section, with an exaggerated conductor thickness for visibility.

The line was realised by adding a second conductor on the backside of the feedline cross-section, as shown in Figure 3.6. The conductor width and the horizontal offsets were swept, trying to bring $Z_o : Z_e$ close to 6 while keeping $v_{po} : v_{pe}$ close to 3. The substrate thickness or channel dimensions were not altered in this study. A coupler is shown in Figure 3.7. The phase velocity ratio was around 2.1.

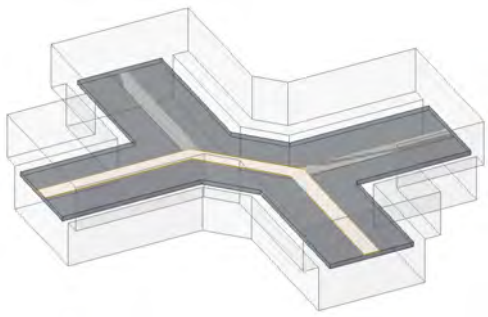

Figure 3.7: Inhomoegenous broadside coupled line coupler.

3.1.6 Inhomogeneous stripline Lange coupler

While experimenting with a Lange coupler [30] in a similar suspended stripline structure, it was observed that the phase velocities of the quasi-odd modes are also very different from the quasi-even modes, behaving similarly to the broadside lines. The initial design was calculated by the design equations provided in [39]. Early results appeared promising, however, due to the relatively complex geometry, there were a very large number of tunable parameters, so only limited optimisation was performed.

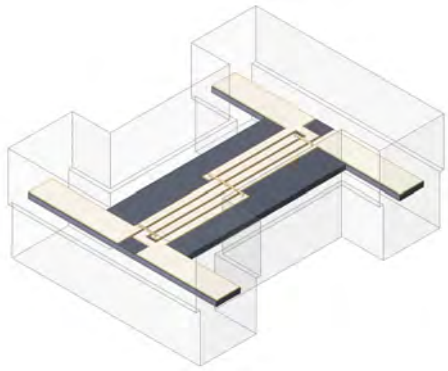

Figure 3.8: Inhomoegenous stripline Lange coupler.

3.1.7 E-plane split blocks

The coupler was designed to be assembled from two parts, a cap and a base, mating on a plane plane along the centre of the broad wall of the waveguide. The larger top-half of the channel allows for some misalignment during assembly, without damaging the membrane. The design of the coupler channel with transitions was transferred to a 3D CAD tool, and the waveguides were extended outwards to the sides of two half-blocks. The waveguides were bent with a large radius while ensuring all 4 lines maintain the same length, before ending in a standard [40] waveguide interface. Guide structures were designed to align the top and bottom blocks. The two block halves are closed by screws.

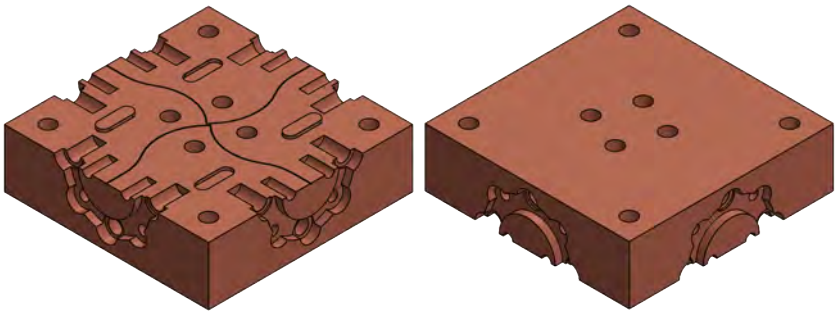

Figure 3.9: E-plane split waveguide blocks for the branch-guide coupler. For detailed drawings, see Appendix B.

3.2 Simulation

The initial circuit-based simulations were performed with a linear circuit simulator, using ideal lossless transmission line models. The junctions were all assumed to be ideal, without any additional parasitics.

All electromagnetic S-parameter simulations were performed using a finite element method (FEM) based 3D electromagnetic field solver. The solver provides a 2D "port-only" solution that calculates the propagation characteristics based on the cross-section geometry of the defined ports. This was used to calculate the fundamental mode impedances and cut-off frequencies of higher-order modes.

For initial simulations, the walls and centre conductors were assigned to be perfect electrical conductor (PEC). As dimensions were tuned and the performance of the hybrids was approaching theoretically predicted behaviour, the boundary conditions were swapped for a more realistic [41] metal conductivity of 2×10^7 S/m. While the actual conductivity of the metals used is likely to be higher than this value, loss due to surface roughness, oxidation and other imperfections can also be modelled as degraded conductivity. The silicon was modelled using a dielectric constant of 11.7 [29] and a loss tangent of 0.0005 [42].

Apart from interactive tuning, parameter sweeps were also used to explore a larger space, for example, when finding impedance ratios for broadside coupled lines. Random-search and gradient based optimisers were used only in the design of the waveguide to stripline transition.

For all data presented in this work, a discrete sweep of 201 frequency points, between 750-1100 GHz, was used, with second-order basis functions. The maximum allowed ΔS between two adaptive passes was set to 0.005. No symmetry planes were used in the simulation. During the course of the project, significantly less expensive solver settings were used to speed up iteration. Most interactive tuning was performed using first order basis functions, ΔS capped to 0.02 and a 51 point discrete sweep. A 11 point sweep, with the same settings, was used for the gradient and random-search optimisers. It was noted that use of interpolating sweeps was particularly ill-suited to these types of structures, often resulting in absurd results.

3.3 Fabrication

The branch-guide coupler was fabricated for characterisation with a VNA.

3.3.1 Machining of waveguide blocks

The blocks were machined in-house by Mr. Jonathan Westin. The material is CW614N standard brass. The smallest inner radius (Appendix A) is 62.5 μm, the deepest slot is 125 μm with a 1:1 aspect ratio, and the narrowest slot is 70 μm. The critical dimensions of the blocks were measured to be within 3 μm of the design.

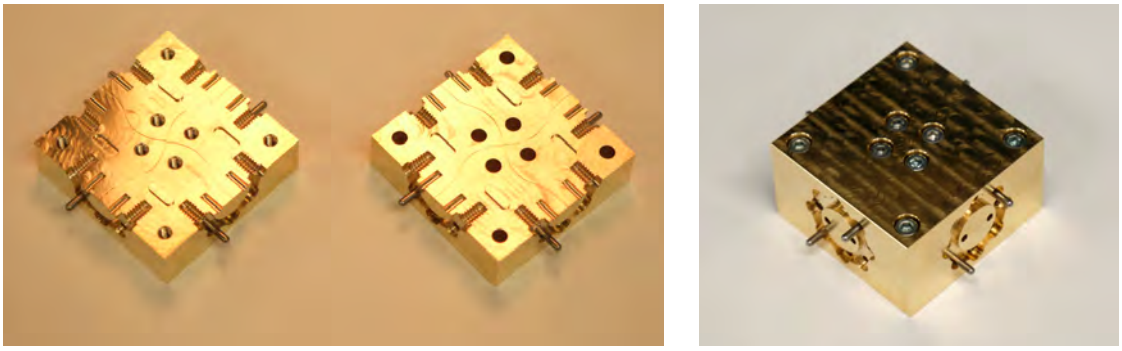

Figure 3.10: Machined E-plane split blocks (left), assembled together (right).

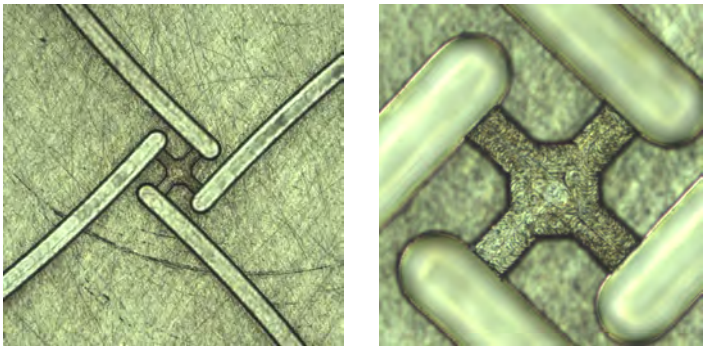

Figure 3.11: Microscope pictures of the base (left) and cap (right) blocks.

3.3.2 Microfabrication of the suspended substrate

The fabrication process for the couplers is based on an SOI wafer comprising of a 3µm device layer, a 1µm buried oxide (BOX) layer, and a 300µm thick handle layer. After dicing the wafer into smaller chips, the couplers are patterned on the handle layer using a bilayer lift-off process. The chip is then flipped and mounted upside down onto a carrier wafer using a temporary wax adhesive. The handle layer is subsequently removed through a combination of dry and wet etching steps. Next, the coupler outline is patterned on backside via photolithography of the remaining thin membrane layer and released by dry etching through the device layer. By dissolving the wax in acetone the couplers are then collected on a filter paper and the remaining photoresist is removed by rinsing in acetone and removers. The circuits

were fabricated in the Nanofabrication Lab at Chalmers, by Mr. Malte Dorneiden, who also developed the process.

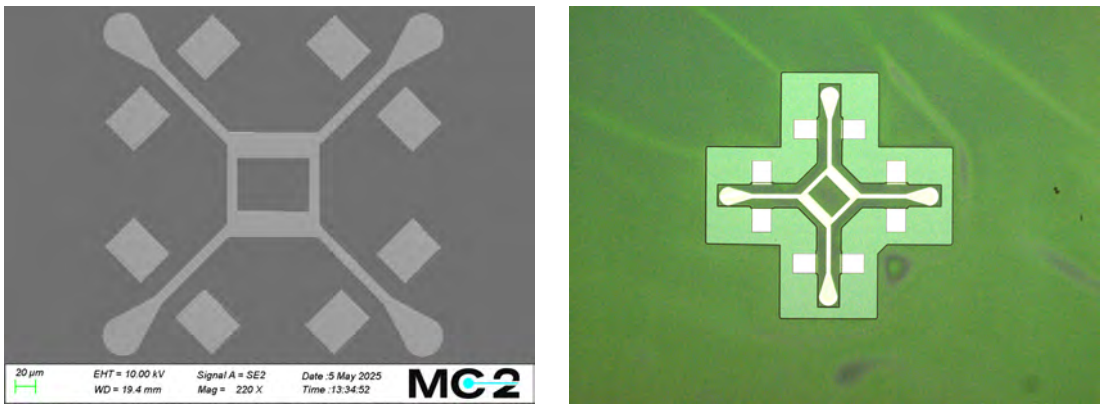

Figure 3.12: SEM image of the front-side patterned metal on the SoI substrate (left) and backside patterning of the substrate (right).

3.3.3 Assembly

The device was assembled with the help of a micro-manipulator, with a fine paint-brush hair used to push the device into place, while a solution of isopropanol and deionized water was used to allow the chip to float.

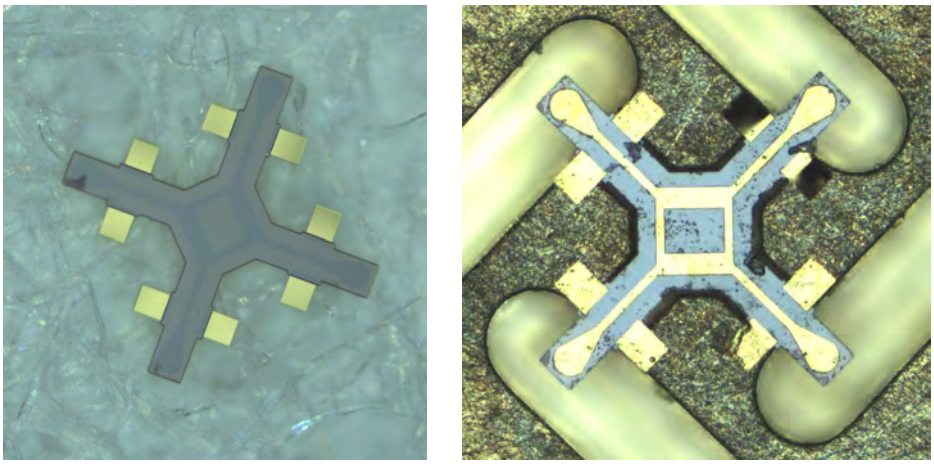

Figure 3.13: Microscope images of a released membrane on filter paper (left) and a mounted membrane (right)

3.4 Characterisation

3.4.1 Measurement setup

S-parameters measurements are performed using a Keysight PNA-X N5242A Vector Network Analyser (VNA), with the N5261A millimetre-wave controller driving a pair of VDI VNAX WR1.0 (WM250) extenders. The rated typical test-port power of the extenders is -23 dBm. The measurements are made with an IF frequency of 100 Hz, without averaging, over 201 frequency points.

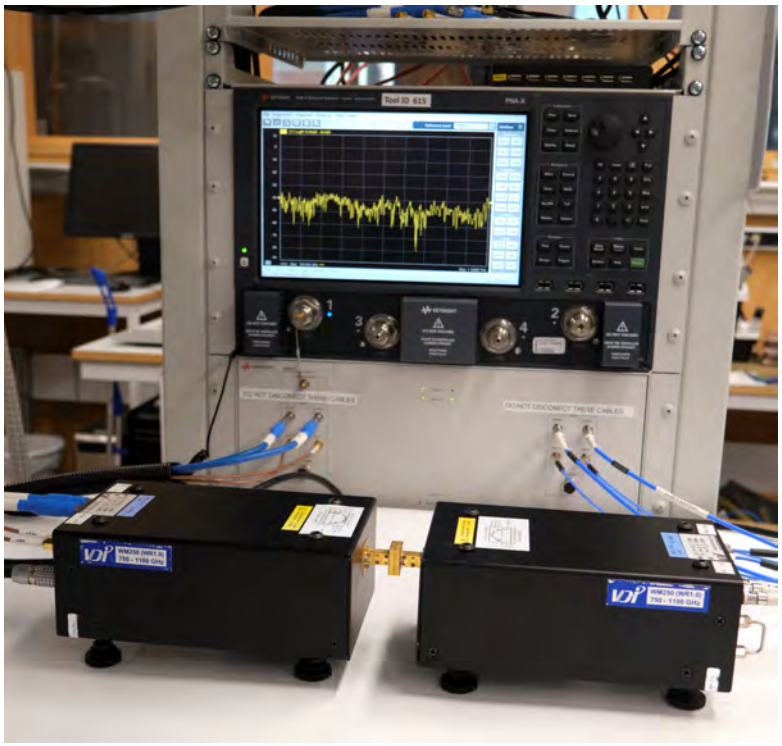

Figure 3.14: The WM-250 waveguide vector measurement setup, for the 750-1100 GHz band.

The data for all measurements is exported from the VNA in Touchstone (s2p) format, which tabulates the real and imaginary parts of each S-parameter, at each frequency point, with a precision of 8 significant figures for each part. The VNA only supports 2 ports, however, this is sufficient to characterize a 4-port network, as long as for each pair of ports, the remaining two ports are terminated. Available horn antennas provide a return loss better than 20 dB, and are used as terminations for measurement.

The VNA is calibrated to the WM-250 flange using the SOLT [43] method. The on-instrument calibration procedure is used. Due to a prevailing issue with one of the two extenders, only one extender is used as the transmitter, thus doubling the number of required measurements. The entire setup is turned on 2 hours prior to calibration, to allow all components in the instrument to reach thermal equilibrium.

Room temperature and humidity are monitored through the measurement. The calibration kit provides a matched load, a short and an quarter-wave offset short. The final "through" reference is measured by directly mating the waveguide flanges of the two extenders, as shown in Figure 3.14. After full calibration, the reflection coefficients of the calibration load, and the termination antennas, are measured and recorded. These reflection coefficients are then re-measured after the completion of the coupler measurement, to ensure that the calibration of the instrument did not drift significantly during the measurement.

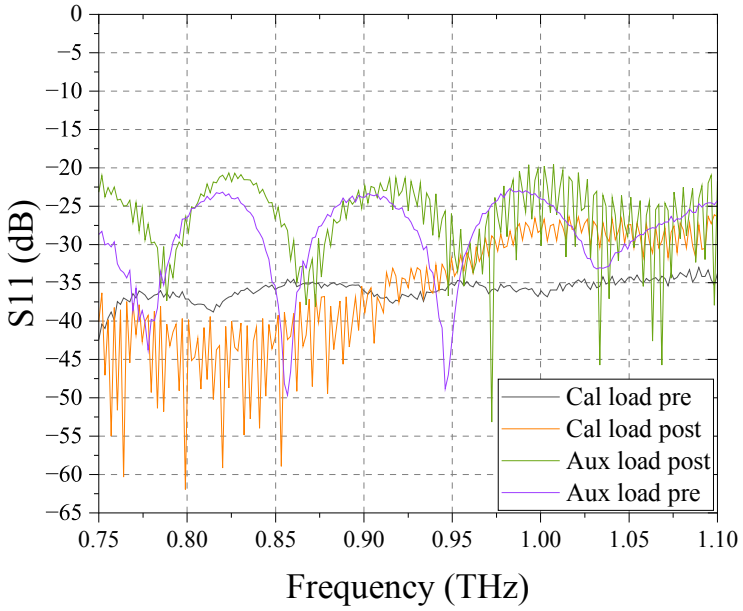

Figure 3.15: Measured reflection coefficient of the calibration and auxiliary loads, pre- and post-measurements. For the duration of measurements, room temperature was 20.5±0.5° C with relative humidity between 44-46%.

4

Results and discussion

In this chapter, the results from the S-parameter simulations and measurements are presented, and the interpretation of this data is briefly discussed.

4.1 Electromagnetic simulations

4.1.1 Branch-guide coupler

The simulations results for the branch-guide coupler are shown below. The results shown below are referenced to the suspended stripline ports (Figure 3.5 (left)), using realistic metal boundaries.

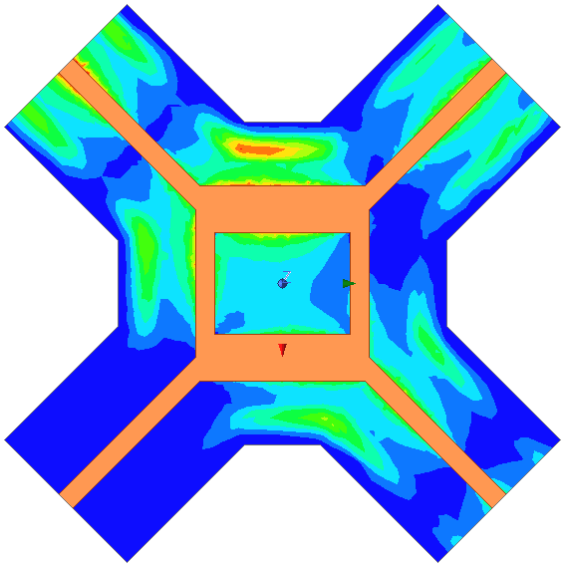

Figure 4.1: *E*-field distribution for an excitation on port 1 of the branch-guide coupler at 925 GHz.

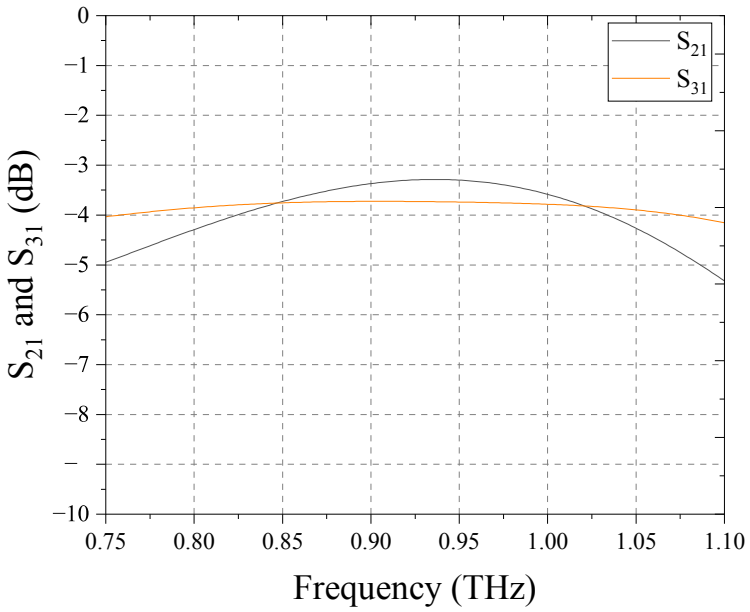

Figure 4.2: Transmission (S_{21}) and coupling (S_{31}) of the branch-guide coupler.

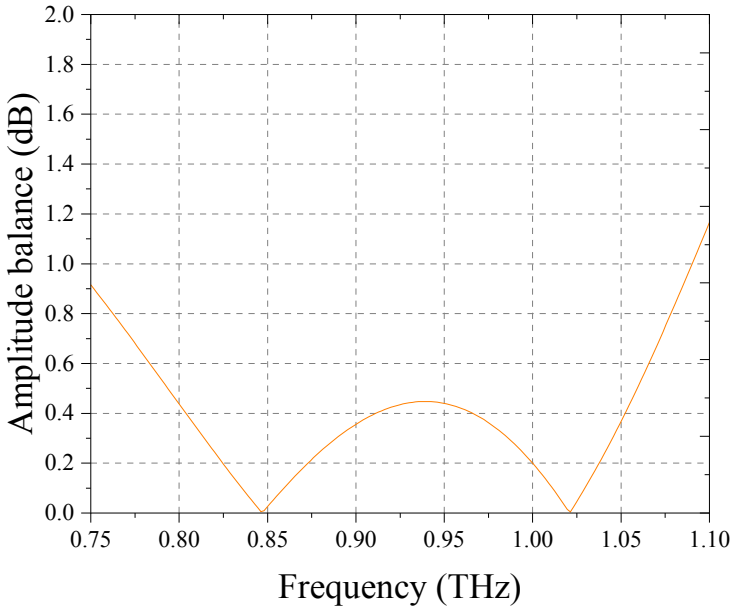

Figure 4.3: Amplitude balance of the branch-guide coupler.

From Figure 4.2, we can see that C approaches 3 dB at the centre frequency of 925 GHz. Figure 4.3 shows that amplitude balance is better than 0.5dB for around 23% bandwidth. For this same bandwidth, the phase balance (Figure 4.4) deviates by 8°.

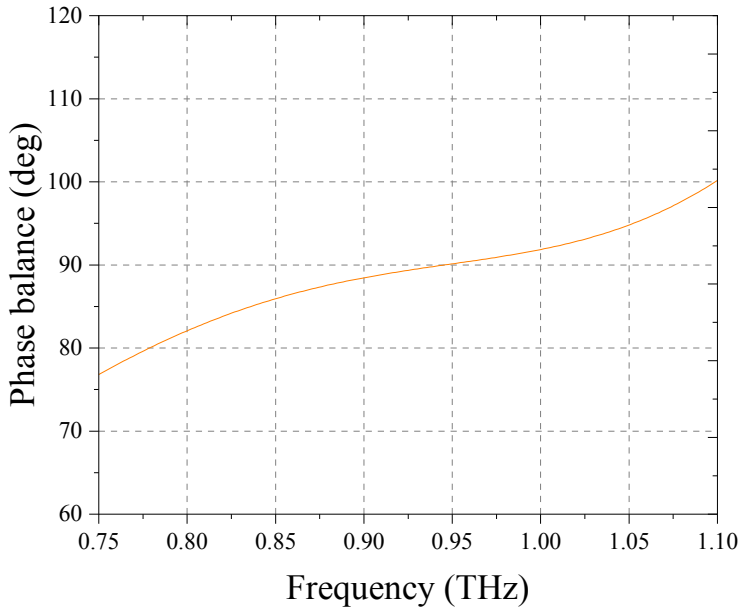

Figure 4.4: Phase balance of the branch-guide coupler.

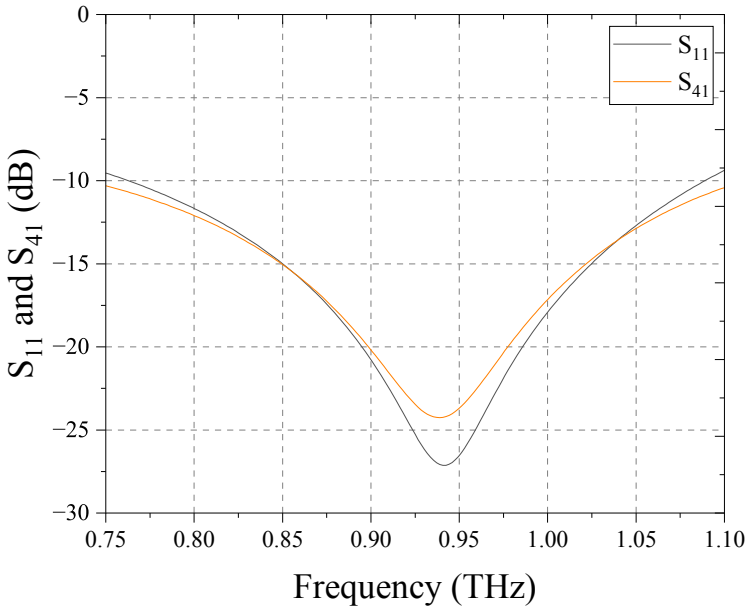

Figure 4.5: Reflection coefficient (S_{11}), and isolation (S_{41}), in the branch-guide coupler.

Figure 4.5 shows that return loss and isolation are better than 15 dB for around 18% bandwidth, which is important for power combining applications. The efficiency factor (Figure 4.6) remains mostly flat through the band.

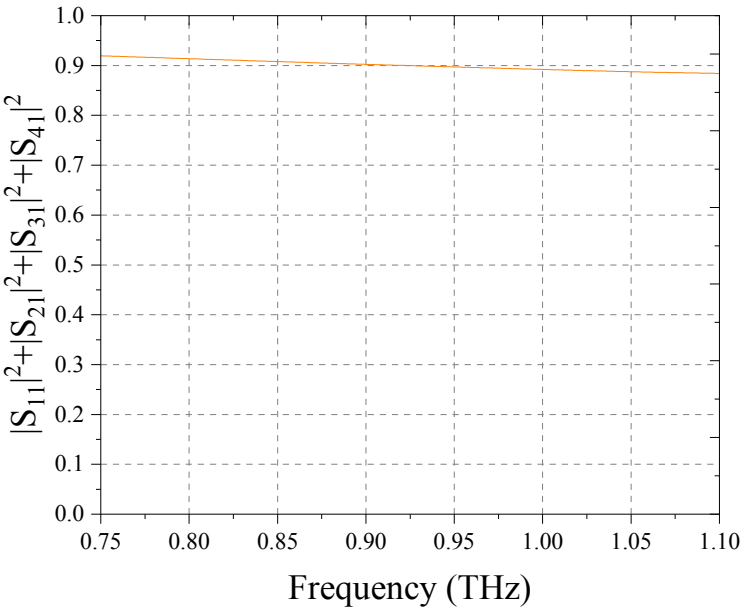

Figure 4.6: Efficiency factor of the branch-guide coupler.

4.1.2 Waveguide transition

The waveguide to suspended stripline transition showed a simulated return loss better than 20 dB, and an insertion loss better than 0.3 dB for the entire WM-250 waveguide band. Thus, it will allow for the couplers to be characterized in a waveguide environment without significantly changing the performance.

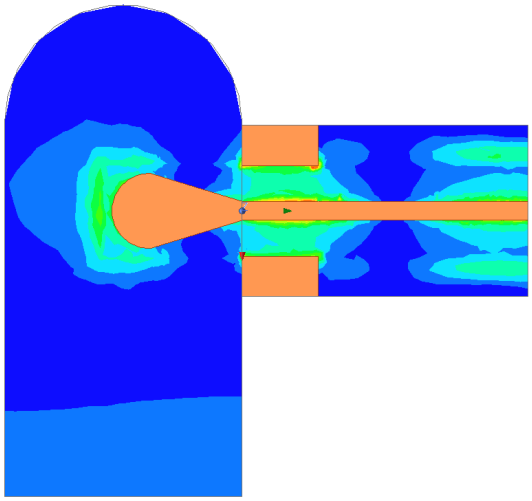

Figure 4.7: *E*-field distribution in the waveguide to suspended stripline transition at 925 GHz.

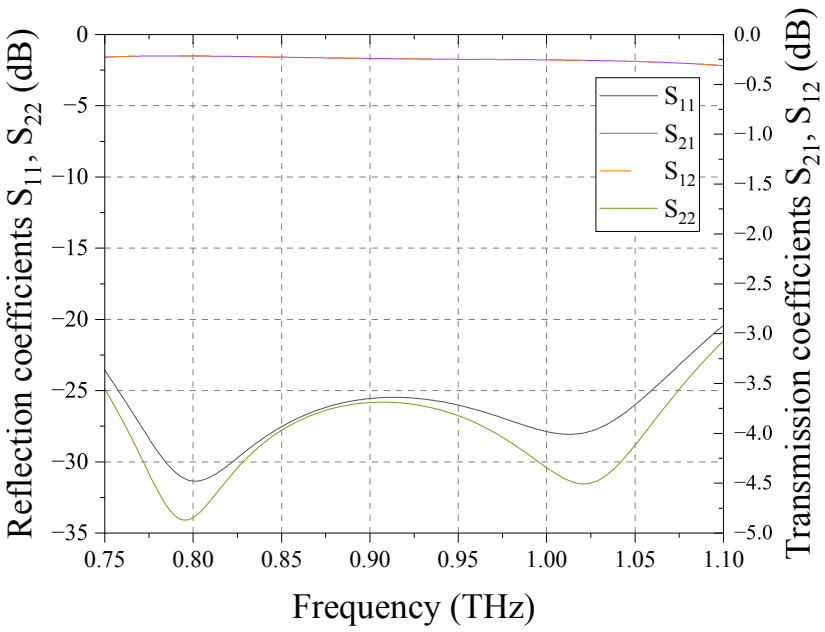

Figure 4.8: Simulated S-parameters of the waveguide to suspended stripline transition.

4.1.3 Branch-guide coupler with waveguide transitions

The simulation results of the branch-guide coupler, embedded in four waveguide-to-suspended-stripline, are presented below. They are referenced to the WM-250 waveguide ports highlighted in Figure 3.5 (right). These simulations results have also been presented in [44].

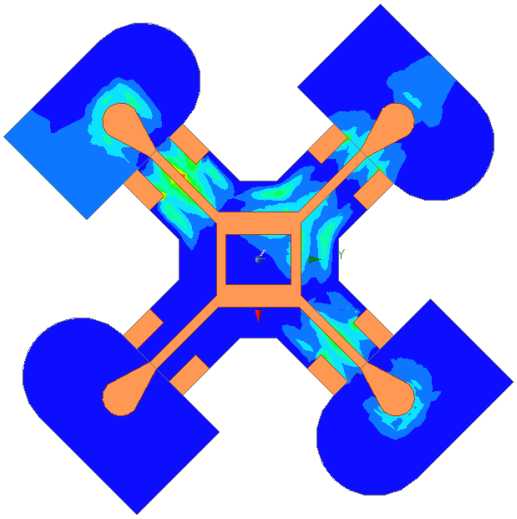

Figure 4.9: *E*-field distribution for an excitation on port 1 of the branch-guide coupler, embedded in transitions, at 925 GHz.

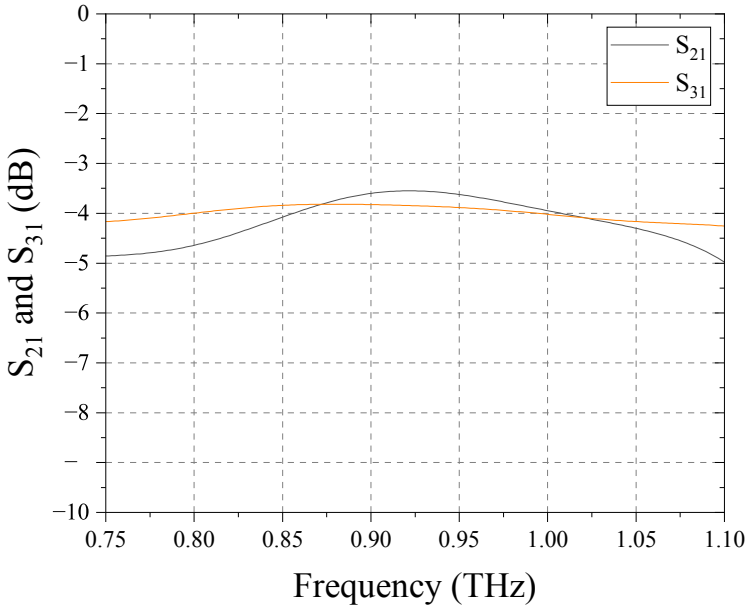

Figure 4.10: Transmission (S_{21}) and coupling (S_{31}) of the branch-guide coupler, embedded in transitions.

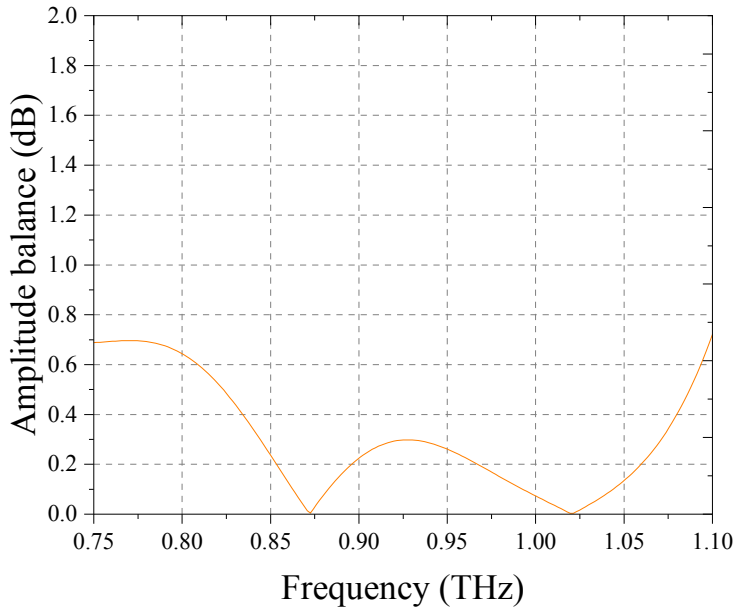

Figure 4.11: Amplitude balance of the branch-guide coupler, embedded in transitions.

The amplitude and phase balance of the embedded coupler clearly vary from the stripline reference plane, but this can be explained by the insertion loss of the transitions.

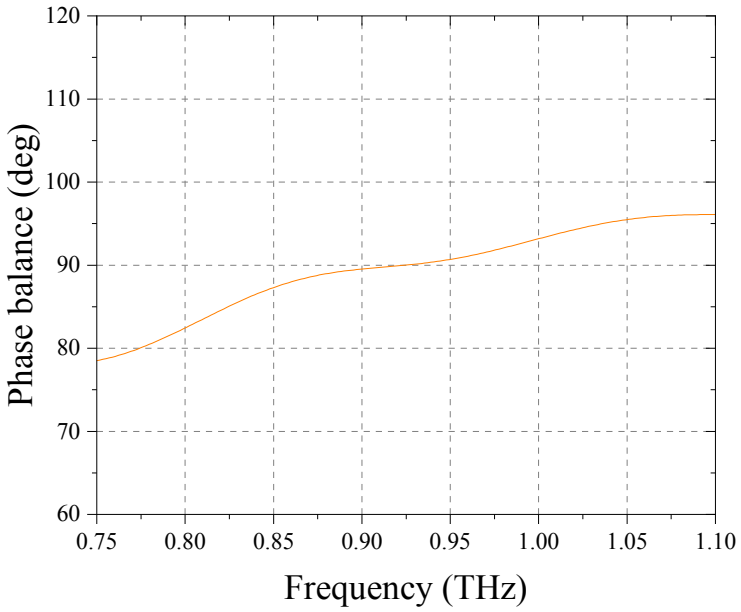

Figure 4.12: Phase balance of the branch-guide coupler, embedded in transitions.

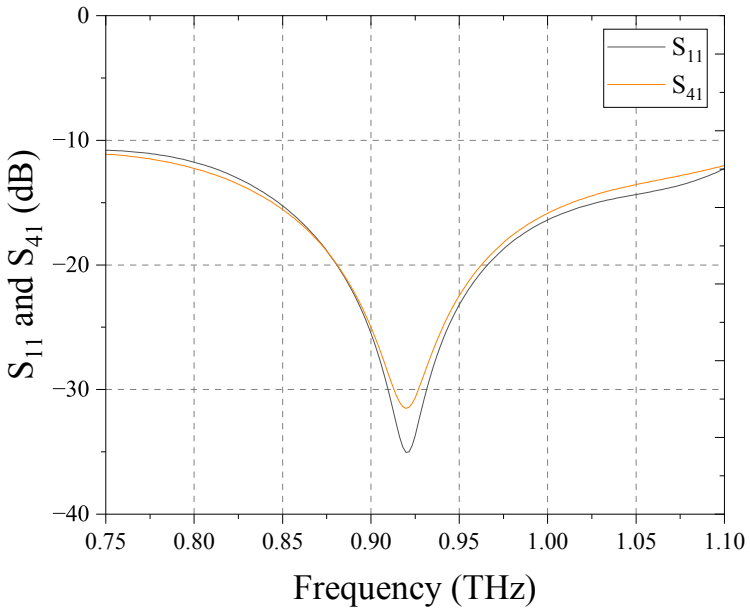

Figure 4.13: Reflection coefficient (S_{11}), and isolation (S_{41}), in the branch-guide coupler, embedded in transitions.

The usable bandwidth remains the same, around 18%. The efficiency factor shows a small dip at the high end of the band, which corresponds to the spike in insertion loss seen in the transition (Figure 4.8).

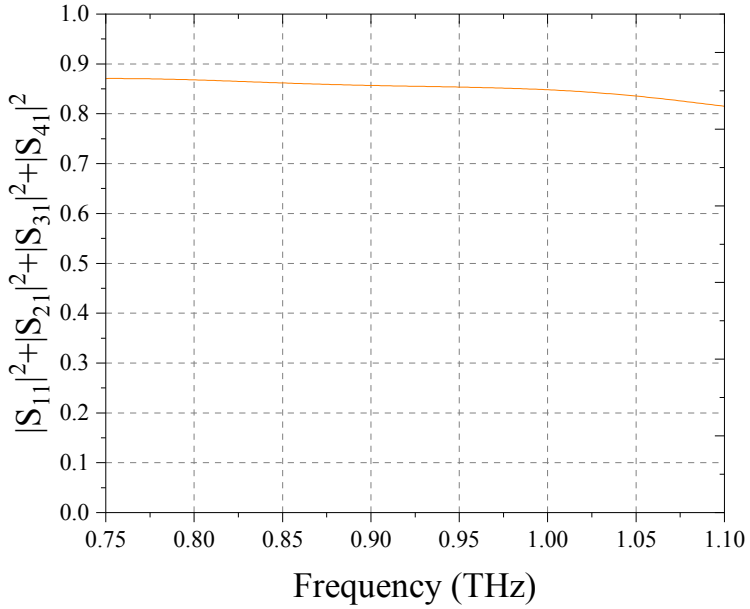

Figure 4.14: Efficiency factor of the branch-guide coupler, embedded in transitions.

4.1.4 Inhomogeneous broadside coupled line coupler

While studying this coupler, dimensions of the substrate and channel were kept fixed to the output of the waveguide transition designed earlier. This resulted in the maximum achieved $v_{pe} : v_{po}$, at the desired $Z_e : Z_o$ ratio of 6, was 2.1. The coupler described by Dalley ideally desires a $v_{pe} : v_{po}$ ratio close to 3. For the fixed channel dimensions, the issue can be visualized in Figure 4.15: when the lines are close to being directly on top of each other, most of the field is forced through the high dielectric substrate. However, due to the dimensions of the channel being large, for a very thin substrate, this results in overcoupling.

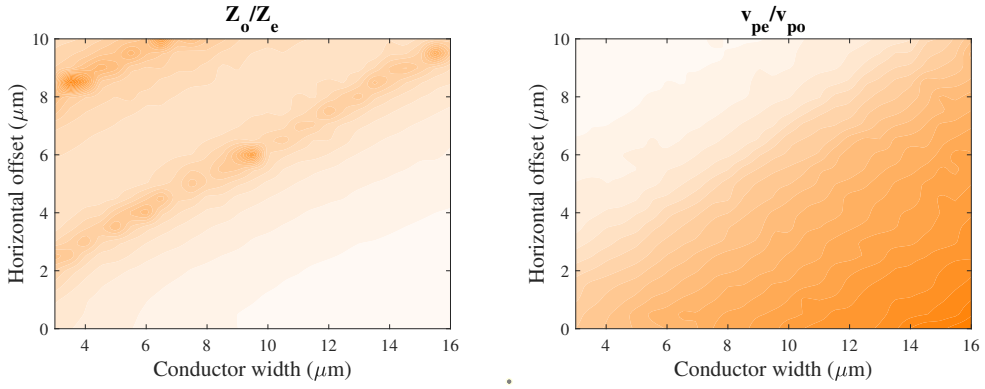

Figure 4.15: Ratios of $Z_e : Z_o$ and $v_{pe} : v_{po}$, swept over the conductor width and horizontal offset for the fixed design channel, where orange represents values closer to 6 and 3, respectively.

Additionally tuning the channel and substrate dimensions can allow the regions of interest to move closer together. As an example, in Figure 4.16, a 10 μm substrate was used with a 40mm base channel, already showing regions with better potential performance. However, due to time constraints, this parameter space was not fully evaluated, as tuning parameters like substrate thickness will need to be evaluated from a mechanical, electromagnetic and fabrication standpoint. A more comprehensive study would likely be able to produce a far more ideal inhomogeneous broadside coupled line.

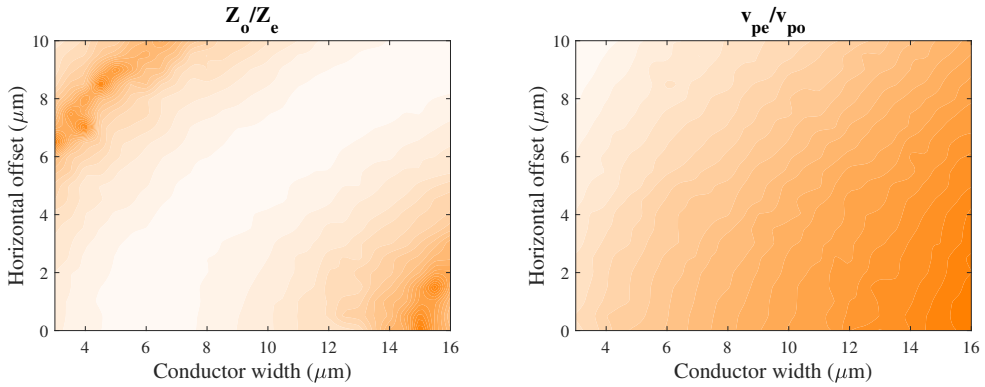

Figure 4.16: Swept ratios of $Z_e : Z_o$ and $v_{pe} : v_{po}$, compared to ideal hybrid values, for a modified channel, showing the ideal regions intersecting.

Even without the ideal coupled line section, the coupler appears promising, especially when low amplitude imbalance over a wide band is desired. The port-flipped behaviour is clearly visible, with the DC-through port behaving as the isolated port.

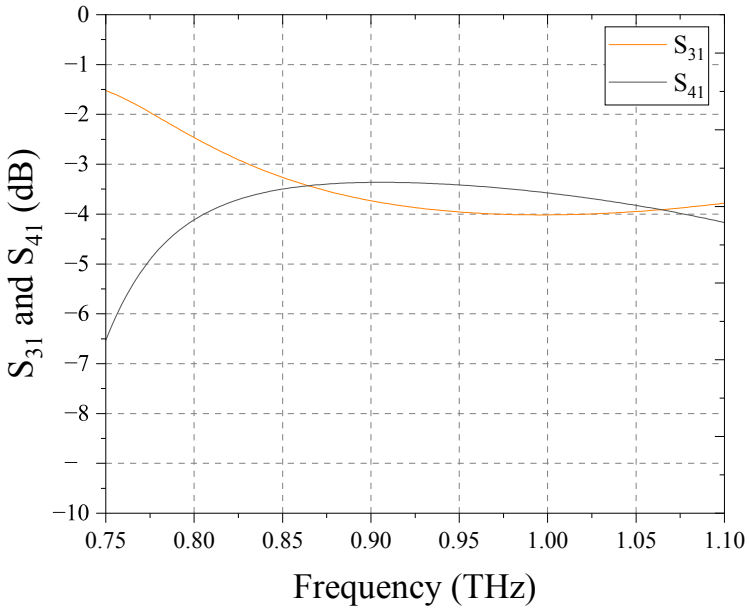

Figure 4.17: Transmission (S_{41}) and coupling (S_{31}) of the inhomogeneous broadside coupled line coupler.

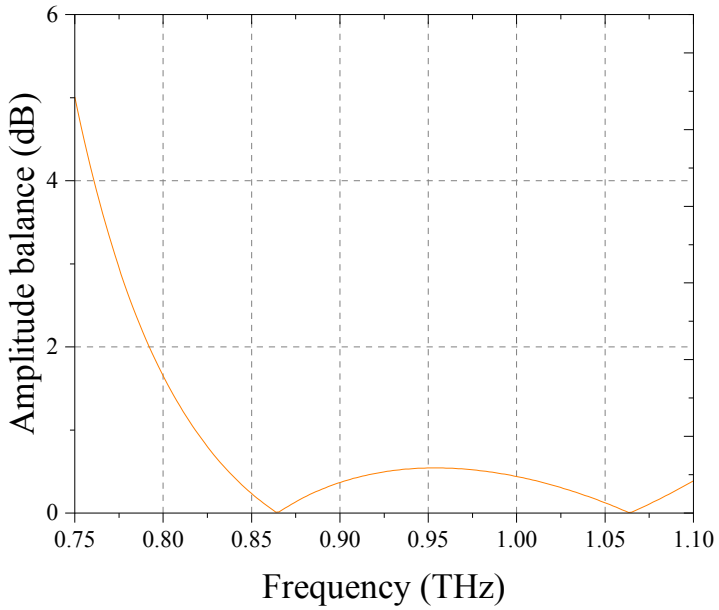

Figure 4.18: Amplitude balance of the inhomogeneous broadside coupled line coupler.

Even when poorly tuned, the phase balance of the inhomogeneous broadside coupled line coupler is better than the other couplers.

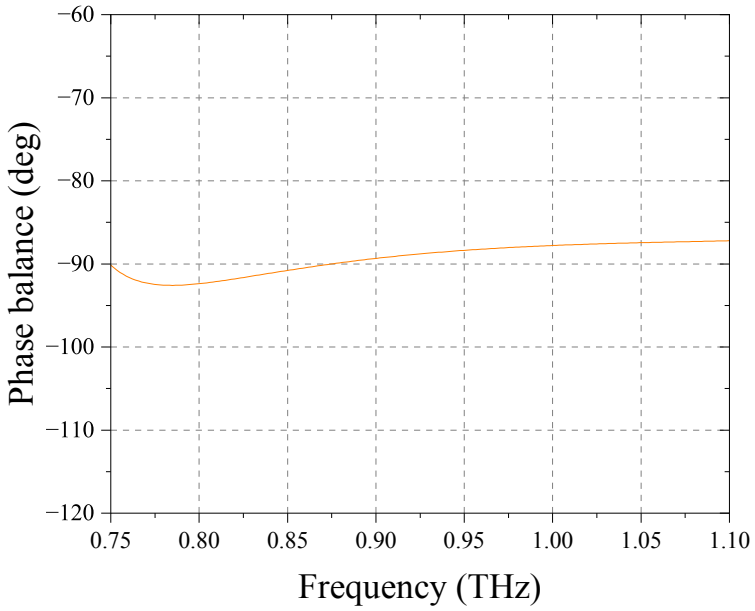

Figure 4.19: Phase balance of the inhomogeneous broadside coupled line coupler.

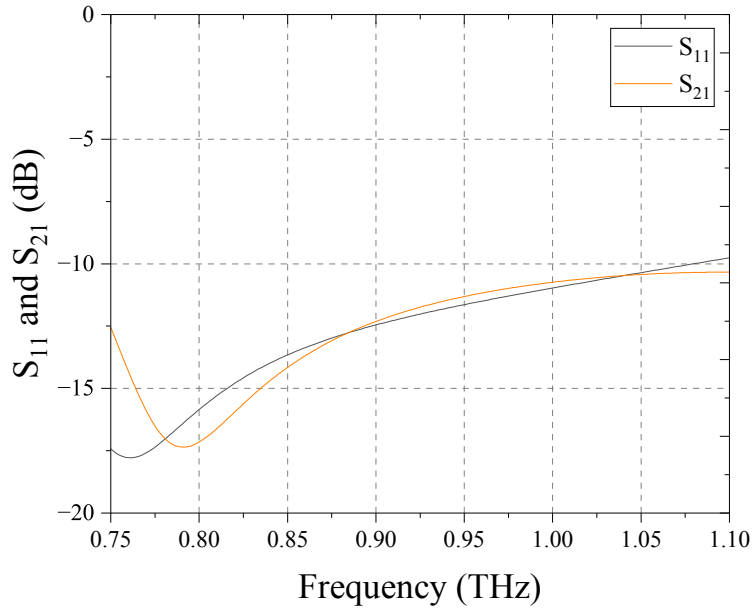

Figure 4.20: Reflection coefficient (S_{11}), and isolation (S_{21}), in the inhomogeneous broadside coupled line coupler.

The efficiency factor is also fairly high, as there are no particularly narrow metal structures causing ohmic loss.

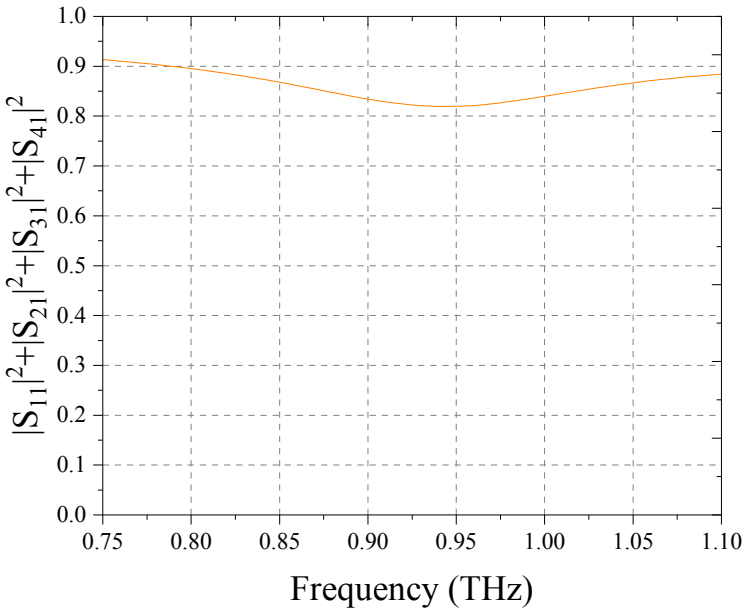

Figure 4.21: Efficiency factor of the inhomogeneous broadside coupled line coupler.

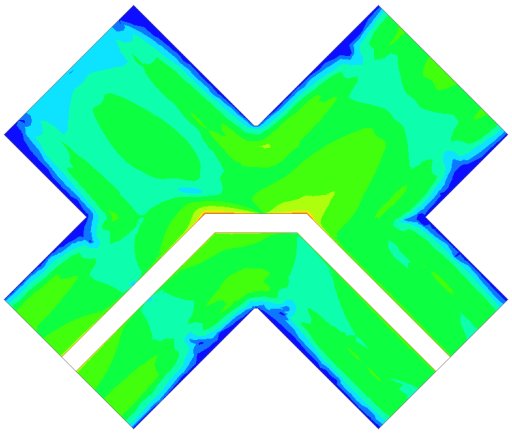

Figure 4.22: *E*-field distribution (top plane) for an excitation on port 1 of the inhomogeneous broadside coupled line coupler at 925 GHz.

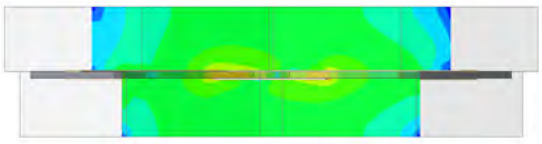

Figure 4.23: *E*-field distribution (side plane) for an excitation on port 1 of the inhomogeneous broadside coupled line coupler at 925 GHz.

4.1.5 Inhomogeneous stripline Lange coupler

The results from initial Lange coupler simulations are presented here as is. A more comprehensive optimization is required to improve the poor performance.

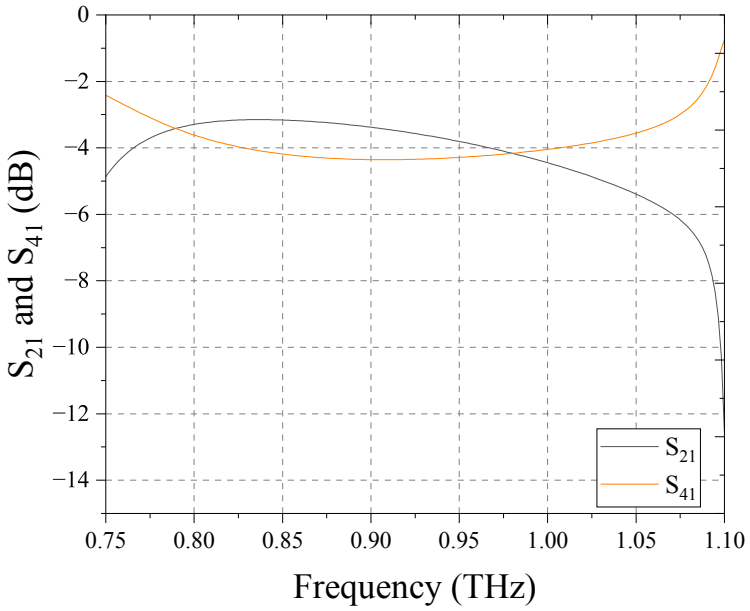

Figure 4.24: Transmission (S_{41}) and coupling (S_{21}) of the Lange coupler.

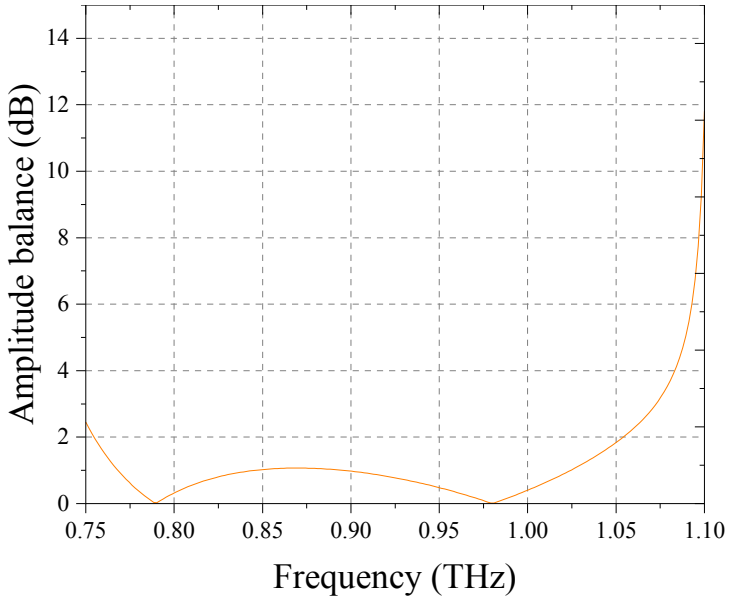

Figure 4.25: Amplitude balance of the Lange coupler.

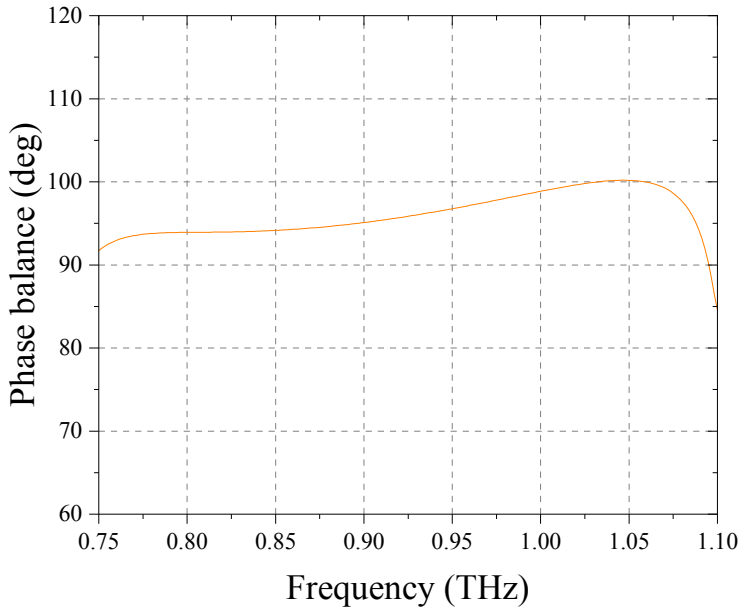

Figure 4.26: Phase balance of the inhomogeneous Lange coupler.

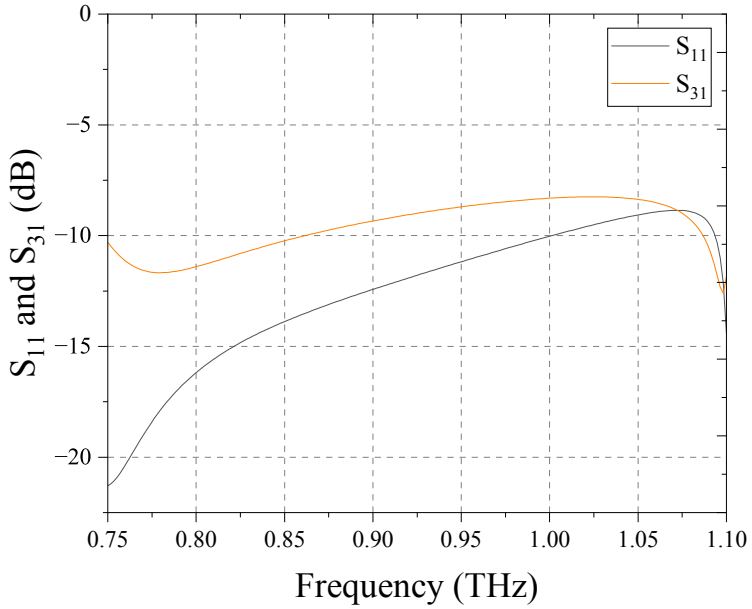

Figure 4.27: Reflection coefficient (S_{11}), and isolation (S_{31}), in the Lange coupler.

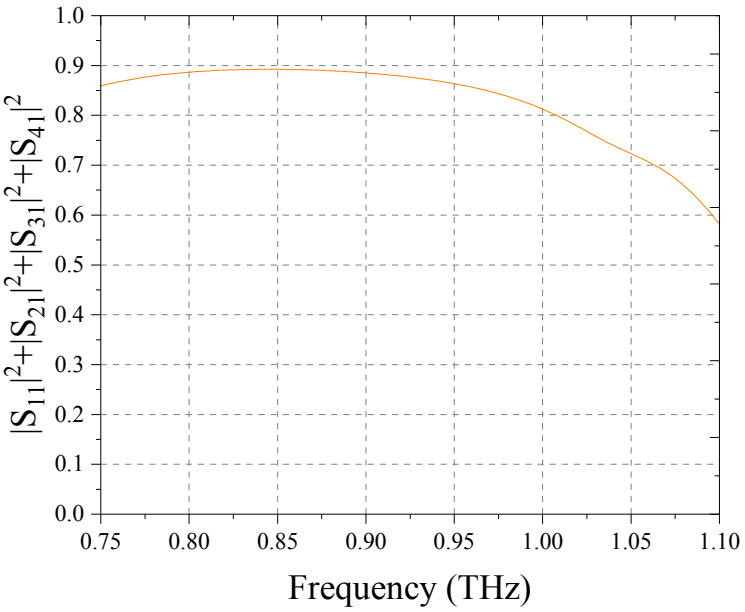

Figure 4.28: Efficiency factor of the inhomogeneous Lange coupler.

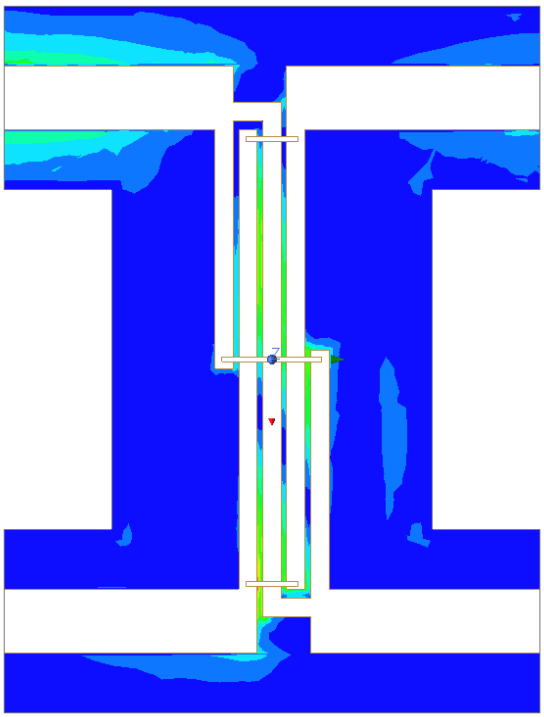

Figure 4.29: *E*-field distribution for an excitation on port 1 of the inhomogeneous Lange coupler at 925 GHz.

In order to understand the behaviour of the fields in the Lange coupler, a cross-section was solved using the 2D port solver, finding that 4 modes could propagate. The fields patterns are shown in Figure 4.30, and Table 4.1 shows the parameters of the modes. It can be seen from these values, that the effective dielectric constant varies significantly between the first three modes, while still remaining being higher than the fourth, even, mode.

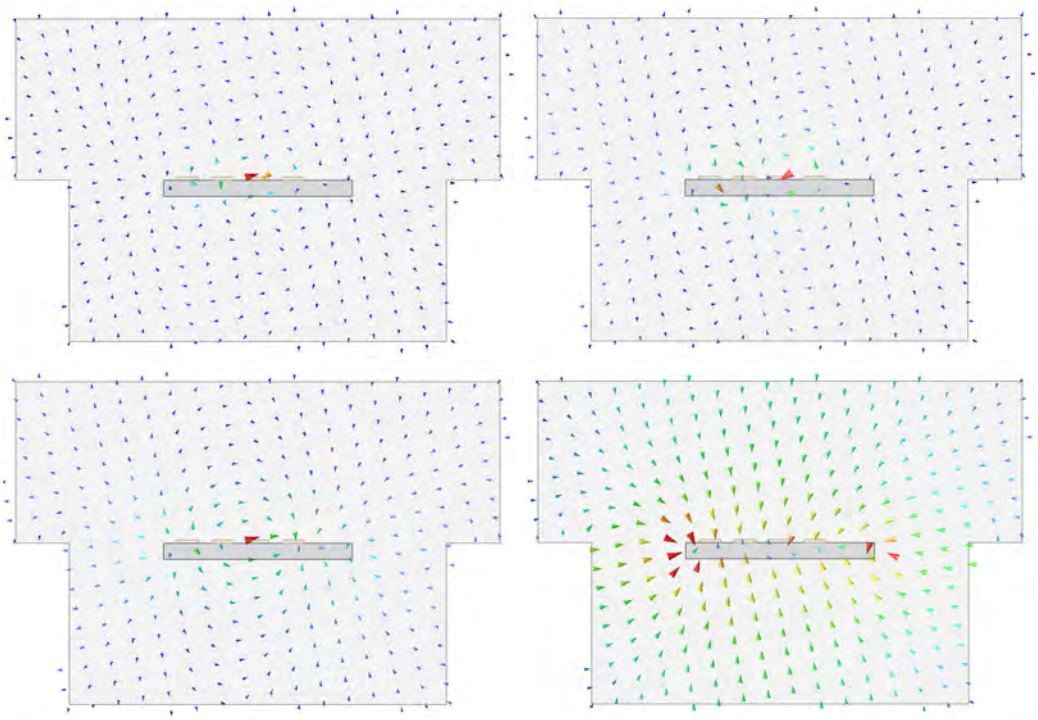

Figure 4.30: The four propagating modes in the cross-section of the Lange coupler.

A potential method to developing this further would be to change the spacing between the outer conductors separately from the spacing between the central conductors, as this may allow the phase velocity difference to be equalized.

Table 4.1: Modes in the Lange cross-section

Mode	Z_0	ϵ_{eff}
1	41	4.9
2	50	4.4
3	224	3.1
4	94	1.2

4.2 Scattering parameter measurements

Measurement results of the branch-guide coupler are presented here. As the coupler can only be measured from the waveguide flange at the edge of the blocks, the extra loss was simulated by changing the waveguide lengths in the transition-embedded model to 18 mm, the same as the blocks. This corresponded to around 4 dB of loss per access waveguide. These waveguide-embedded simulation results are presented along with the measurements, as a reference. All presented measurements are for excitations on the same physical port, designated port 1.

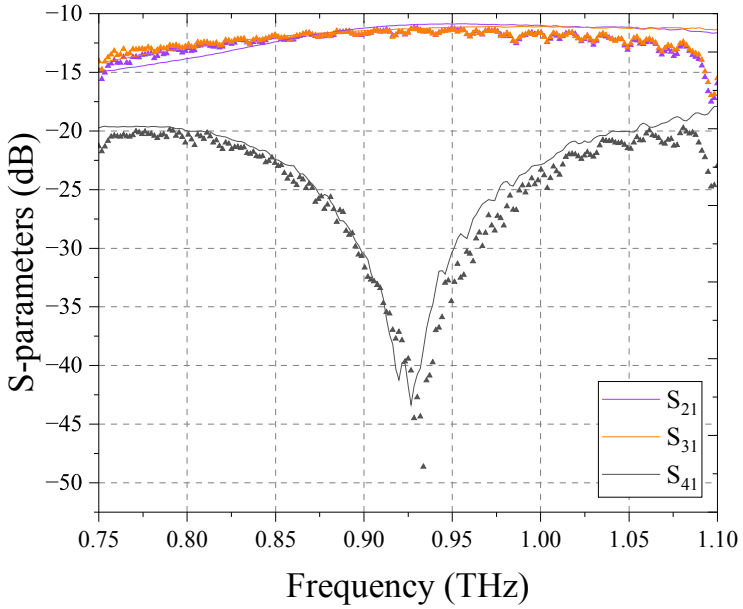

Figure 4.31: Transmission (S_{21}), coupling (S_{31}) and isolation (S_{41}) for excitations on port 1. Triangles are measured data points, solid lines represent the simulation results for the flange reference plane.

From Figure 4.31, the through, coupled and isolated ports' behaviours appear to closely match the simulation results. The centre frequency also appears to be close to the simulated model. Amplitude balance (Figure 4.32) appears better than simulated. The reflection coefficient (Figure 4.33) appears high, however, this is likely not representative of the reflection coefficient of the coupler itself, but rather is dominated by either poor calibration, or the mismatch at the flange [45]. The large access waveguides with their loss prevent accurate characterization of return loss of the coupler. Efficiency factor (Figure 4.34) indicates that there are no unexpected large losses.

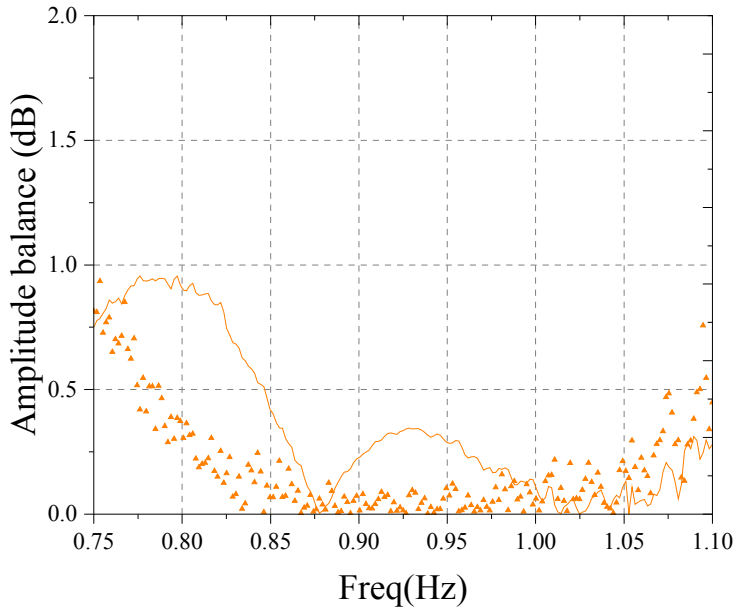

Figure 4.32: Amplitude balance for excitation on port 1. Triangles are measured data points, solid lines represent the simulation results for the flange reference plane.

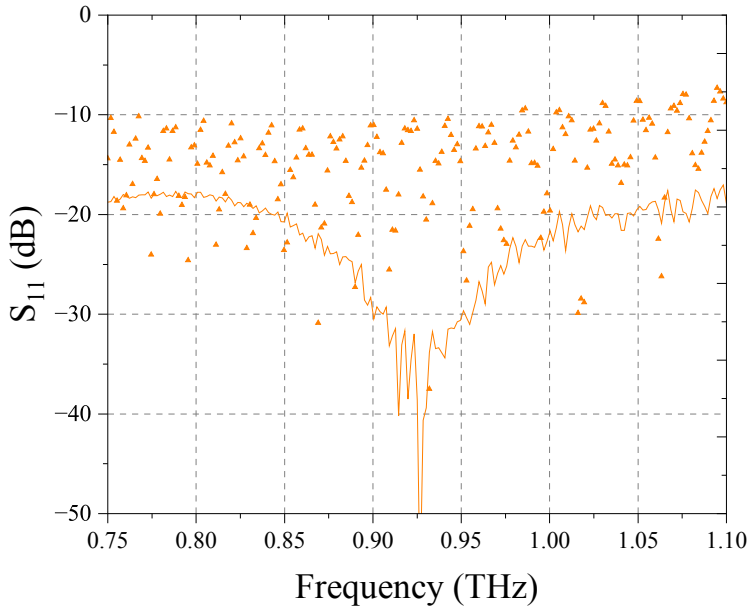

Figure 4.33: Reflection coefficient of port 1, with other ports terminated. Triangles are measured data points, solid lines represent the simulation results for the flange reference plane.

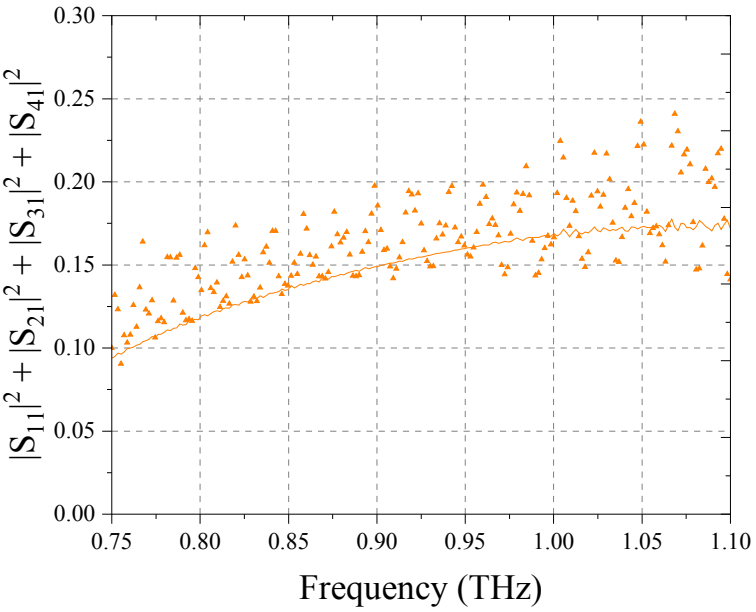

Figure 4.34: Efficiency factor for port 1 excitation. Triangles are measured data points, solid lines represent the simulation results for the flange reference plane.

5

Conclusion

This thesis began as an exploration of terahertz hybrid designs, with the tentative goal of producing a full-waveguide-band hybrid for WM-250. After the initial literature survey, the early attempts were simply to try what appeared to be the obvious solution - to synthesize branch-guide hybrids. In this process, however, the limitations of these hybrids became apparent. Fabricating low impedance lines was difficult, and limited the number of sections, and achievable bandwidth was effectively capped. Published designs [18] [19] were already at the limit of what is possible by machining, and while microfabrication techniques [46] could push the branch-guide coupler a bit further, they added a great deal of complexity, and alignment still remained a major challenge. It became apparent that there is a need to explore alternate technologies, to design hybrids that scale far further into the terahertz gap. The choice of a planar technology was natural - most mixer diodes at these frequencies are already designed to operate in shielded channels, and the waveguide-to-suspended-stripline transitions are already integrated into these mixer membranes. Integrating the hybrid onto the membrane would add minimal extra processing.

The preliminary measurement results for the branch-line coupler are promising, and more comprehensive measurements are underway. The simulations for the Lange and inhomogeneous coupled lines are incomplete. However, it is apparent that there exists a massive parameter space and there is a lot of potential performance still to be unlocked. As a part of fabricating the membrane, a backside patterning process was developed to define the membrane itself. This process must now be extended further, to perform backside lift-off, allowing for broadside-coupled lines, as well as potentially through-via backside jumpers for the Lange design.

The back-to-back waveguide-coupled block, while important for characterization, is not a very useful device. One of the most common uses of hybrids at these frequencies is to drive balanced and sideband separating mixers. Even relatively low-performance hybrids can achieve fairly high sideband suppressing ratios [47]. From the branch-line hybrid's simulated performance, sideband suppressing ratios of 25 dB to 30 dB are possible, over an 18% bandwidth. The real potential of the couplers proposed in this thesis would be in the integration of mixer diode circuits.

Bibliography

[1] E. Wilkinson, "An N-Way Hybrid Power Divider," *IEEE Transactions on Microwave Theory and Techniques*, vol. 8, no. 1, pp. 116–118, Jan. 1960, 70. DOI: 10.1109/TMTT.1960.1124668.

[2] S. Cohn and R. Levy, "History of Microwave Passive Components with Particular Attention to Directional Couplers," *IEEE Transactions on Microwave Theory and Techniques*, vol. 32, no. 9, pp. 1046–1054, Sep. 1984, 10. DOI: 10.1109/TMTT.1984.1132816.

[3] H. A. Bethe, "Theory of Diffraction by Small Holes," *Physical Review*, vol. 66, no. 7-8, pp. 163–182, Oct. 1944, 20. DOI: 10.1103/PhysRev.66.163.

[4] W. Tyrrell, "Hybrid Circuits for Microwaves," *Proceedings of the IRE*, vol. 35, no. 11, pp. 1294–1306, Nov. 1947, 30. DOI: 10.1109/JRPROC.1947.233572.

[5] L. Young, "Branch guide directional couplers," *Proceedings of the National Electronics Conference*, vol. 12, pp. 723–732, 1956, 32.

[6] S. Rehnmark, "Wide-Band Balanced Line Microwave Hybrids," *IEEE Transactions on Microwave Theory and Techniques*, vol. 25, no. 10, pp. 825–830, Oct. 1977, 60. DOI: 10.1109/TMTT.1977.1129221.

[7] S. Cohn, "Shielded Coupled-Strip Transmission Line," *IEEE Transactions on Microwave Theory and Techniques*, vol. 3, no. 5, pp. 29–38, Oct. 1955, 49. DOI: 10.1109/TMTT.1955.1124973.

[8] E. Jones, "Coupled-Strip-Transmission-Line Filters and Directional Couplers," *IEEE Transactions on Microwave Theory and Techniques*, vol. 4, no. 2, pp. 75–81, Apr. 1956, 40. DOI: 10.1109/TMTT.1956.1125022.

[9] S. Cohn, "Characteristic Impedances of Broadside-Coupled Strip Transmission Lines," *IEEE Transactions on Microwave Theory and Techniques*, vol. 8, no. 6, pp. 633–637, Nov. 1960, 50. DOI: 10.1109/TMTT.1960.1124809.

[10] A. R. Kerr, "Elements for E-Plane Split-Block Waveguide Circuits," *ALMA Memo 381*, Jul. 2001.

[11] J. Cabello-Sánchez, V. Drakinskiy, J. Stake, and H. Rodilla, "A Capacitive-Gap Coupled Terahertz Planar-Goubau-Line Power Divider," *IEEE Transactions on Terahertz Science and Technology*, vol. 13, no. 6, pp. 698–703, Nov. 2023, 90. DOI: 10.1109/TTHZ.2023.3303849.

[12] S. Srikanth and A. R. Kerr, "Waveguide Quadrature Hybrids for ALMA Receivers," *ALMA Memo 343*, Jan. 2001.

[13] T. Bryllert, V. Drakinskiy, K. B. Cooper, and J. Stake, "Integrated 200–240-GHz FMCW Radar Transceiver Module," *IEEE Transactions on Microwave*

Theory and Techniques, vol. 61, no. 10, pp. 3808–3815, Oct. 2013, 105. DOI: 10.1109/TMTT.2013.2279359.

[14] J. Reed, "The Multiple Branch Waveguide Coupler," *IRE Transactions on Microwave Theory and Techniques*, vol. 6, no. 4, pp. 398–403, Oct. 1958, 132. DOI: 10.1109/TMTT.1958.1125213.

[15] R. Levy and L. Lind, "Synthesis of Symmetrical Branch-Guide Directional Couplers," *IEEE Transactions on Microwave Theory and Techniques*, vol. 16, no. 2, pp. 80–89, Feb. 1968, 134. DOI: 10.1109/TMTT.1968.1126612.

[16] B. Z. Balázs, N. Geier, M. Takács, and J. P. Davim, "A review on micro-milling: Recent advances and future trends," *The International Journal of Advanced Manufacturing Technology*, vol. 112, no. 3-4, pp. 655–684, Jan. 2021, 140. DOI: 10.1007/s00170-020-06445-w.

[17] X. Hao et al., "Fabrication of large aspect ratio pcd micro-milling tool with pulsed lasers and grinding," *Journal of Manufacturing Processes*, vol. 58, pp. 489–499, 2020. DOI: https://doi.org/10.1016/j.jmapro.2020.08.032.

[18] A. Khudchenko et al., "Design and Performance of a Sideband Separating SIS Mixer for 800–950 GHz," *IEEE Transactions on Terahertz Science and Technology*, vol. 9, no. 6, pp. 532–539, Nov. 2019, 110. DOI: 10.1109/TTHZ.2019.2939003.

[19] P. J. Sobis, J. Stake, and A. Emrich, "A 170 GHz 45° Hybrid for Submillimeter Wave Sideband Separating Subharmonic Mixers," *IEEE Microwave and Wireless Components Letters*, vol. 18, no. 10, pp. 680–682, Oct. 2008, 120. DOI: 10.1109/LMWC.2008.2003463.

[20] H. Rashid, V. Desmaris, V. Belitsky, M. Ruf, T. Bednorz, and A. Henkel, "Design of Wideband Waveguide Hybrid With Ultra-Low Amplitude Imbalance," *IEEE Transactions on Terahertz Science and Technology*, vol. 6, no. 1, pp. 83–90, Jan. 2016, 142. DOI: 10.1109/TTHZ.2015.2502070.

[21] C. Jung-Kubiak et al., "A Multistep DRIE Process for Complex Terahertz Waveguide Components," *IEEE Transactions on Terahertz Science and Technology*, pp. 1–6, 2016, 145. DOI: 10.1109/TTHZ.2016.2593793.

[22] J. Svedin, R. Malmqvist, B. Beuerle, U. Shah, and J. Oberhammer, "A 230–300 GHz low-loss micromachined waveguide hybrid coupler," in *2017 47th European Microwave Conference (EuMC)*, 155, Nuremberg: IEEE, Oct. 2017, pp. 616–619, ISBN: 978-2-87487-047-7. DOI: 10.23919/EuMC.2017.8230923.

[23] V. Desmaris, D. Meledin, A. Pavolotsky, and V. Belitsky, "Microfabrication Technology for All-Metal Sub-mm and THz Waveguide Receiver Components," *19th International Symposium on Space Terahertz Technology*, Apr. 2008.

[24] R. Monje, V. Belitsky, and V. Vassilev, "A novel design of broadband waveguide directional couplers and 3-dB hybrids," in *2006 IEEE MTT-S International Microwave Symposium Digest*, ISSN: 0149-645X, Jun. 2006, pp. 1169–1172. DOI: 10.1109/MWSYM.2006.249399.

[25] L. Zeng et al., "A Silicon Chip-Based Waveguide Directional Coupler for Terahertz Applications," *IEEE Transactions on Terahertz Science and Technology*, vol. 10, no. 6, pp. 698–703, Nov. 2020, 162. DOI: 10.1109/TTHZ.2020.3022018.

[26] J. L. Hesler and A. W. Lichtenberger, "THz waveguide couplers using quartz micromachining," *21st International Symposium on Space Terahertz Technology*, Jan. 2010.

[27] "IEEE Standard for Rectangular Metallic Waveguides and Their Interfaces for Frequencies of 110 GHz and Above—Part 1: Frequency Bands and Waveguide Dimensions," *IEEE Std 1785.1-2012*, pp. 1–22, 2013. DOI: 10.1109/IEEESTD.2013.6471987.

[28] J. Dalley, "A Strip-Line Directional Coupler Utilizing a Non-Homogeneous Dielectric Medium," *IEEE Transactions on Microwave Theory and Techniques*, vol. 17, no. 9, pp. 706–712, Sep. 1969, 170. DOI: 10.1109/TMTT.1969.1127039.

[29] M. A. Green and M. J. Keevers, "Optical properties of intrinsic silicon at 300 k," *Progress in Photovoltaics: Research and Applications*, vol. 3, no. 3, pp. 189–192, 1995. DOI: https://doi.org/10.1002/pip.4670030303. eprint: https://onlinelibrary.wiley.com/doi/pdf/10.1002/pip.4670030303.

[30] J. Lange, "Interdigitated Stripline Quadrature Hybrid (Correspondence)," *IEEE Transactions on Microwave Theory and Techniques*, vol. 17, no. 12, pp. 1150–1151, Dec. 1969, 180. DOI: 10.1109/TMTT.1969.1127115.

[31] R. E. Collin, "Passive microwave devices," in *Foundations for Microwave Engineering*. 2001, pp. 394–480. DOI: 10.1109/9780470544662.ch6.

[32] L. Young, "Branch guide directional couplers," *Proc. Nat. Electronics Conf.*, vol. 12, pp. 723–732, 1956.

[33] J. Reed and G. Wheeler, "A method of analysis of symmetrical four-port networks," *IRE Transactions on Microwave Theory and Techniques*, vol. 4, no. 4, pp. 246–252, 1956. DOI: 10.1109/TMTT.1956.1125071.

[34] R. E. Collin, "Circuit theory for waveguiding systems," in *Foundations for Microwave Engineering*. 2001, pp. 220–302. DOI: 10.1109/9780470544662.ch4.

[35] D. Frickey, "Conversions between s, z, y, h, abcd, and t parameters which are valid for complex source and load impedances," *IEEE Transactions on Microwave Theory and Techniques*, vol. 42, no. 2, pp. 205–211, 1994. DOI: 10.1109/22.275248.

[36] R. Marks and D. Williams, *A general waveguide circuit theory*, Oct. 1992. DOI: https://doi.org/10.6028/jres.097.024.

[37] S. A. Schelkunoff, "Impedance concept in wave guides," *Quarterly of Applied Mathematics*, vol. 2, no. 1, pp. 1–15, 1944.

[38] J. W. Kooi et al., "A full-height waveguide to thin-film microstrip transition with exceptional RF bandwidth and coupling efficiency," *International Journal of Infrared and Millimeter Waves*, vol. 24, no. 3, pp. 261–284, Mar. 1, 2003. DOI: 10.1023/A:1021903132609.

[39] D. M. Pozar, *Microwave engineering*, 4th ed. Hoboken, NJ: Wiley, 2012, 732 pp., OCLC: ocn714728044, ISBN: 978-0-470-63155-3.

[40] "IEEE Standard for Rectangular Metallic Waveguides and Their Interfaces for Frequencies of 110 GHz and Above—Part 2: Waveguide Interfaces," *IEEE Std 1785.2-2016*, pp. 1–22, 2016. DOI: 10.1109/IEEESTD.2016.7564020.

[41] N. Laman and D. Grischkowsky, "Terahertz conductivity of thin metal films," *Applied Physics Letters*, vol. 93, no. 5, p. 051 105, Aug. 2008. DOI: 10.1063/1.2968308.

[42] D. Grischkowsky, S. Keiding, M. van Exter, and C. Fattinger, "Far-infrared time-domain spectroscopy with terahertz beams of dielectrics and semiconductors," *J. Opt. Soc. Am. B*, vol. 7, no. 10, pp. 2006–2015, Oct. 1990. DOI: 10.1364/JOSAB.7.002006.

[43] W. Kruppa and K. Sodomsky, "An explicit solution for the scattering parameters of a linear two-port measured with an imperfect test set (correspondence)," *IEEE Transactions on Microwave Theory and Techniques*, vol. 19, no. 1, pp. 122–123, 1971. DOI: 10.1109/TMTT.1971.1127466.

[44] A. Goturu, M. Dorneiden, and J. Stake, "A planar 925-ghz branch line coupler," in *To be presented at the 2025 50th International Conference on Infrared, Millimeter, and Terahertz Waves (IRMMW-THz)*, 2025.

[45] D. Bannister, E. Griffin, and T. Hodgetts, *On the dimensional tolerances of rectangular waveguide for reflectometry at millimetric wavelengths*. National Physical Laboratory, 1989.

[46] A. Pavolotsky, D. Meledin, C. Risacher, M. Pantaleev, and V. Belitsky, "Micromachining approach in fabricating of THz waveguide components," *Microelectronics Journal*, European Micro and Nano Systems, vol. 36, no. 7, pp. 683–686, Jul. 1, 2005. DOI: 10.1016/j.mejo.2005.04.041.

[47] P. J. Sobis, A. Emrich, and J. Stake, "A low VSWR 2sb schottky receiver," *IEEE Transactions on Terahertz Science and Technology*, vol. 1, no. 2, pp. 403–411, Nov. 2011. DOI: 10.1109/TTHZ.2011.2166176.

[48] *VDI UG387-M Precision Waveguide Interface*. [Online]. Available: https://www.vadiodes.com/images/AppNotes/VDI_UG387-M_PRECISION_WAVEGUIDE_INTERFACE_R4V6_21-05-04_CUSTOMER_DRAWING.pdf.

A

Appendix: Mechanical drawings of E-plane split block

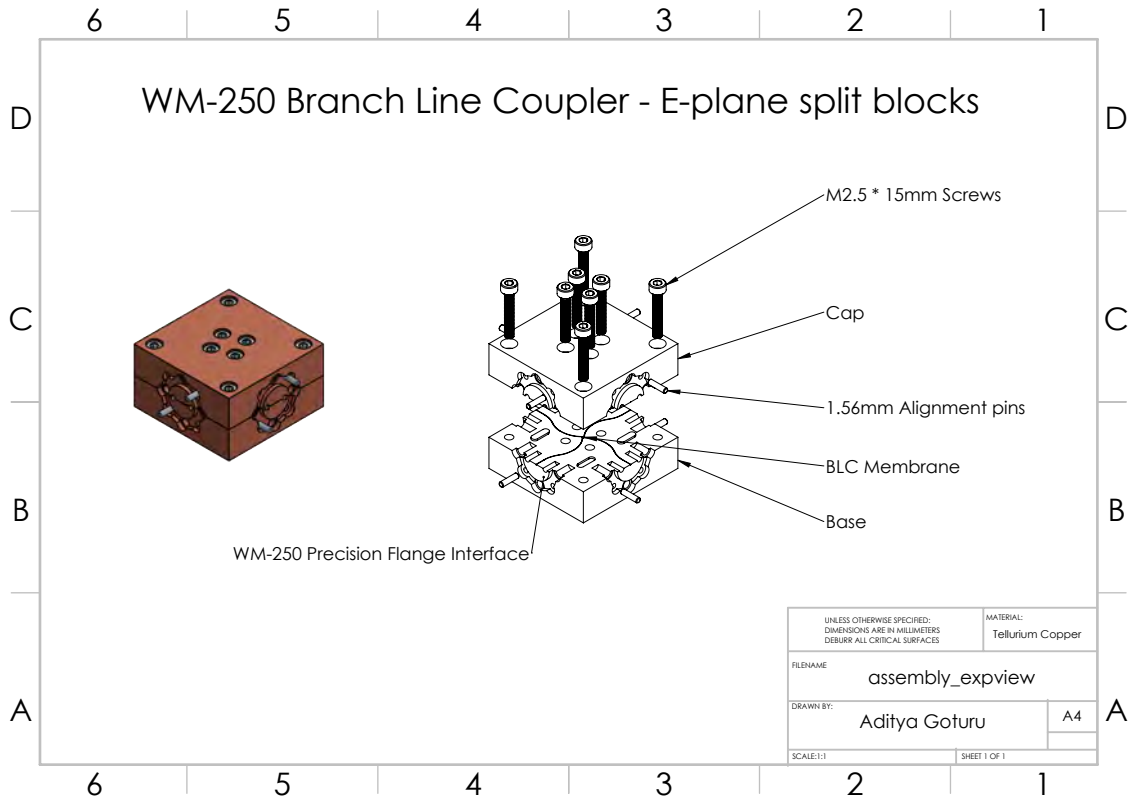

Overview of E-plane split blocks for branch line coupler. For flange specification, refer to [48].

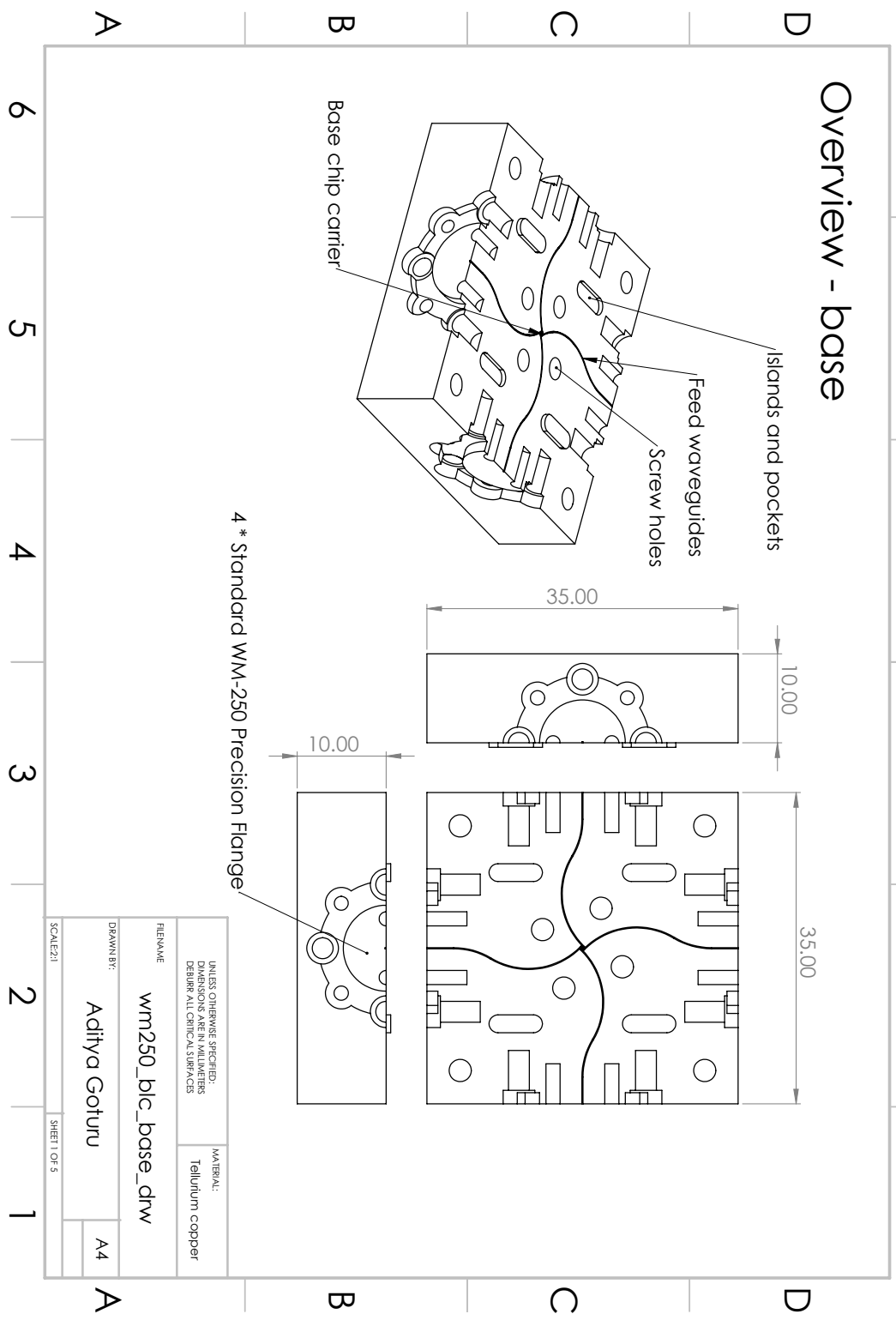
Overview - base
Base chip carrier
Islands and pockets
Feed waveguides
Screw holes
4 * Standard WM-250 Precision Flange
35.00
10.00
10.00
35.00
UNLESS OTHERWISE SPECIFIED:
DIMENSIONS ARE IN MILLIMETERS
DEBURR ALL CRITICAL SURFACES
MATERIAL:
Tellurium copper
FILENAME
wm250_blc_base_drw
DRAWN BY:
Aditya Goturu
A4
SCALE:2:1
SHEET 1 OF 5

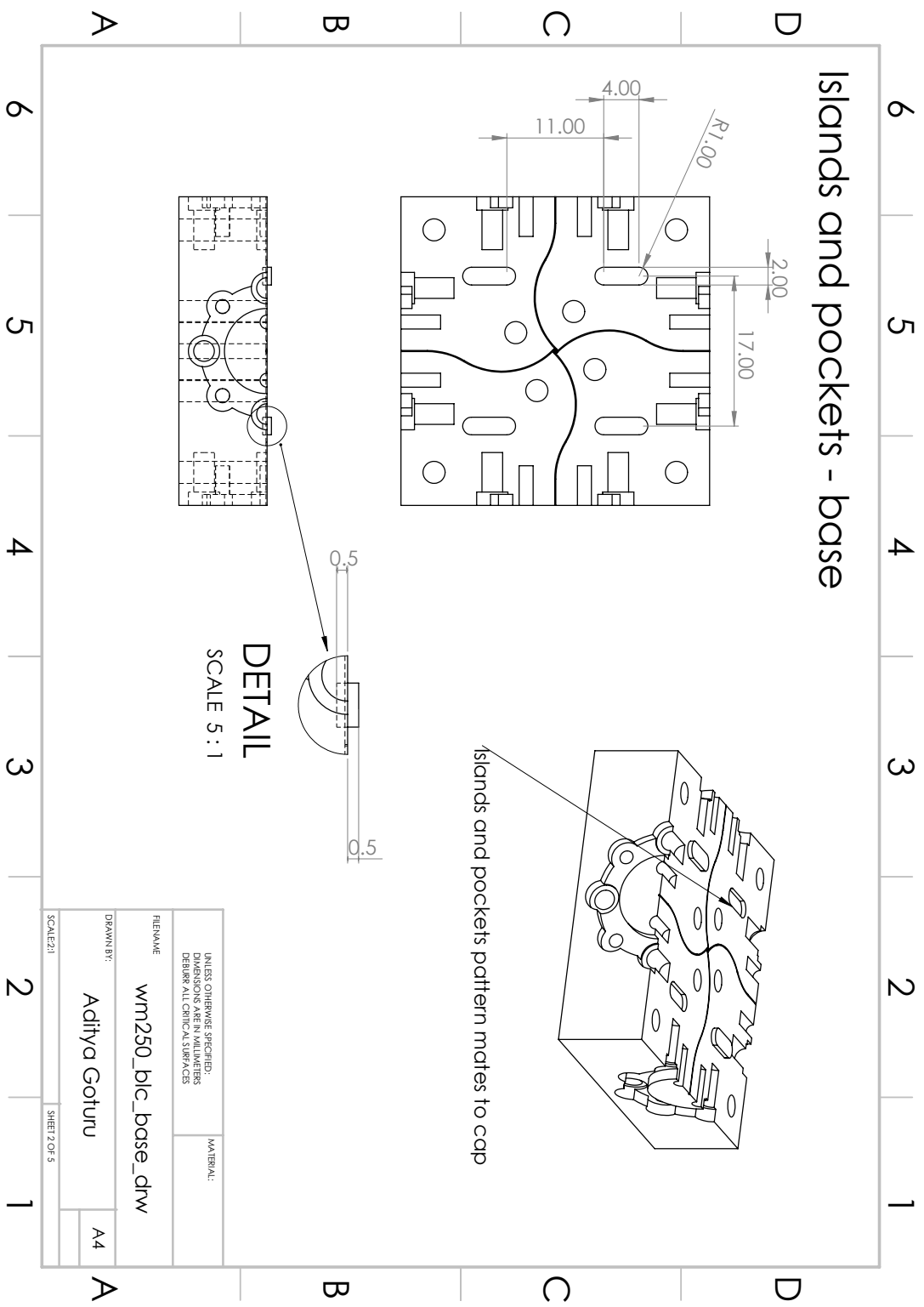
Islands and pockets - base
4.00
11.00
R1.00
2.00
17.00
DETAIL
SCALE 5 : 1
0.5
0.5
Islands and pockets pattern mates to cap
UNLESS OTHERWISE SPECIFIED:
DIMENSIONS ARE IN MILLIMETERS
DEBURR ALL CRITICAL SURFACES
MATERIAL:
FILENAME
wm250_blc_base_drw
DRAWN BY:
Aditya Goturu
A4
SCALE:2:1
SHEET 2 OF 5

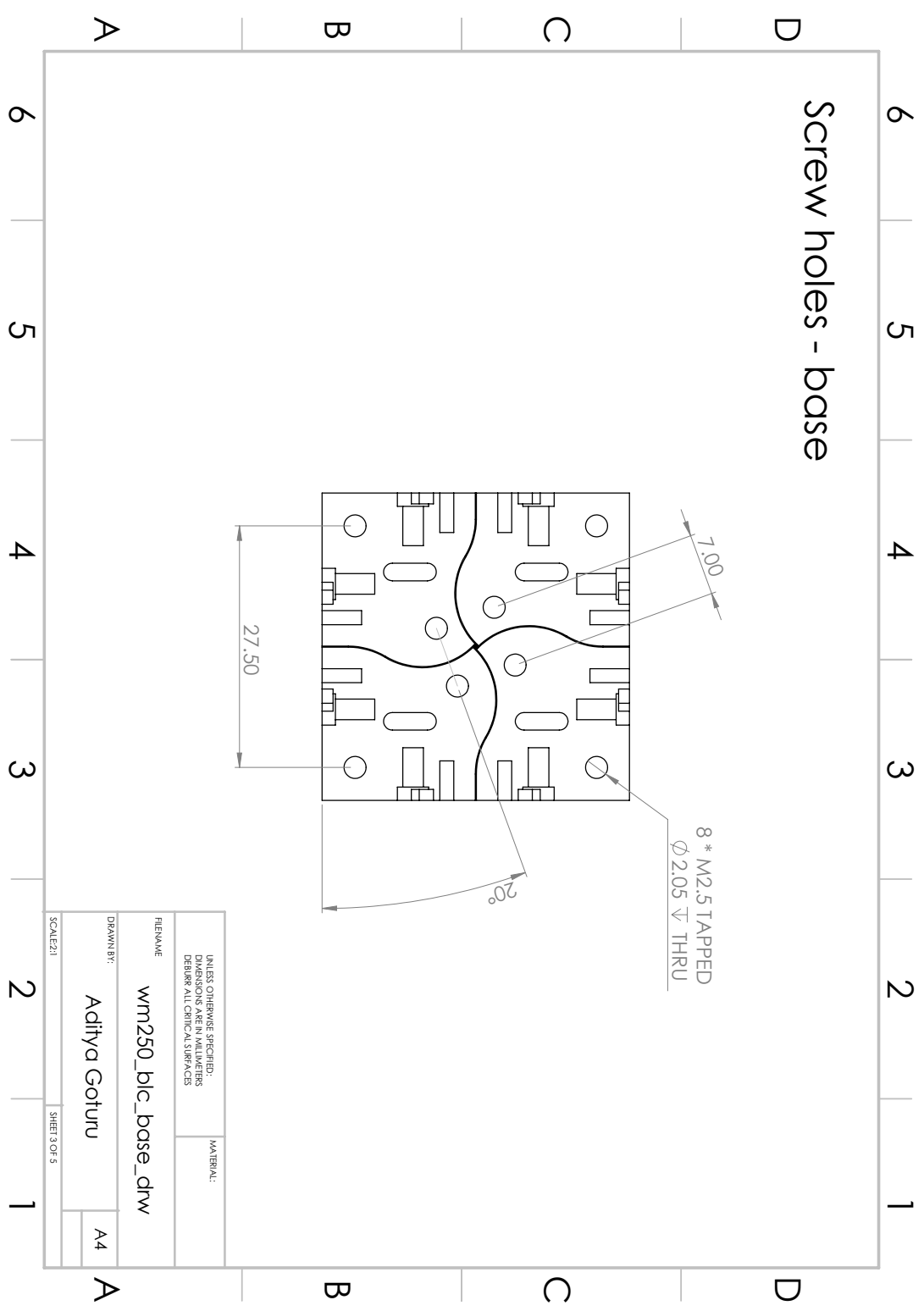
Screw holes - base
7.00
27.50
8 * M2.5 TAPPED
Ø 2.05 ↓ THRU
20°
UNLESS OTHERWISE SPECIFIED:
DIMENSIONS ARE IN MILLIMETERS
DEBURR ALL CRITICAL SURFACES
MATERIAL:
FILENAME
wm250_blc_base_drw
DRAWN BY:
Aditya Goturu
A4
SCALE:2:1
SHEET 3 OF 5

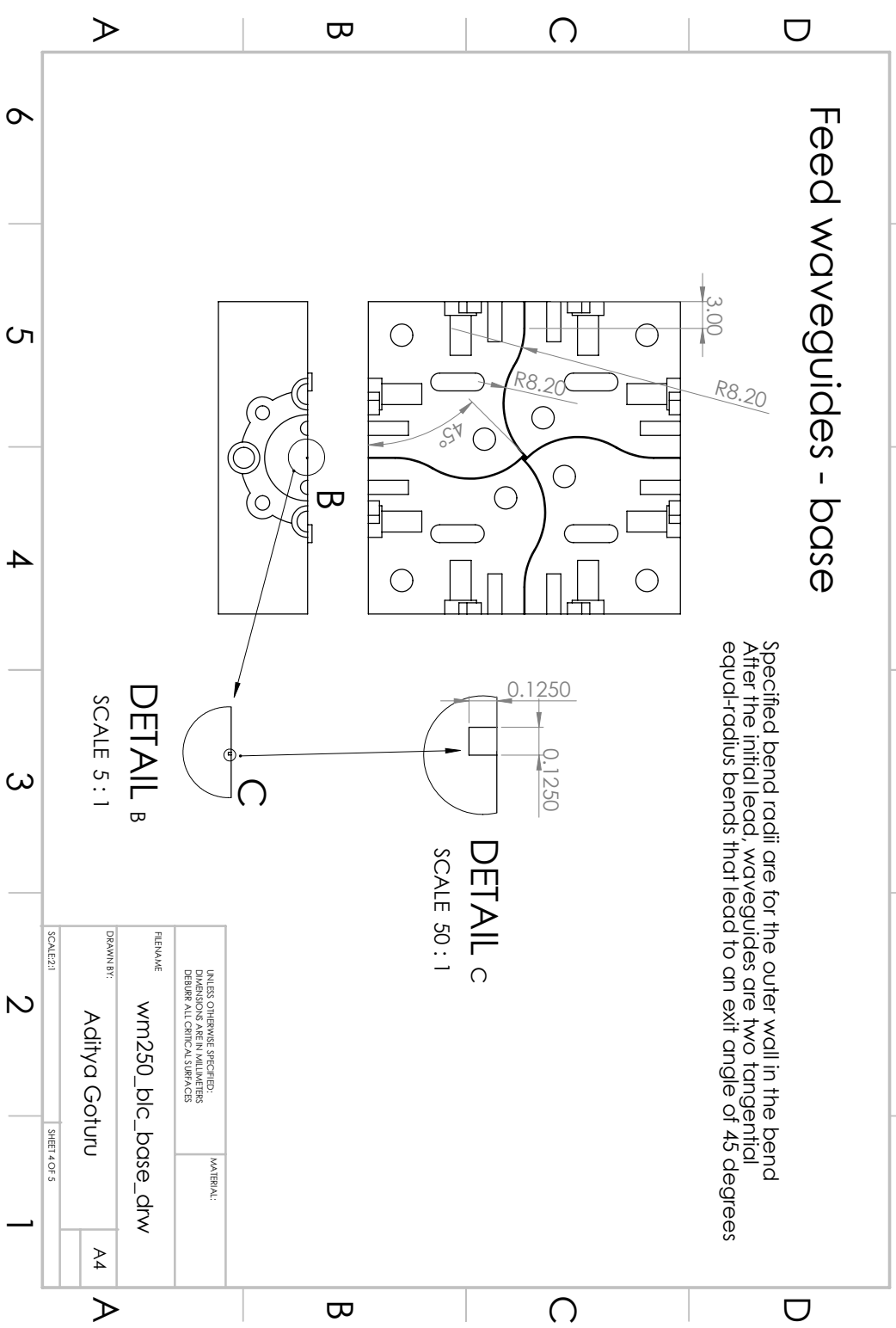
Feed waveguides - base
3.00
R8.20
R8.20
45°
Specified bend radii are for the outer wall in the bend
After the initial lead, waveguides are two tangential
equal-radius bends that lead to an exit angle of 45 degrees
DETAIL B
SCALE 5 : 1
DETAIL C
SCALE 50 : 1
0.1250
0.1250
UNLESS OTHERWISE SPECIFIED:
DIMENSIONS ARE IN MILLIMETERS
DEBURR ALL CRITICAL SURFACES
MATERIAL:
FILENAME
wm250_blc_base_drw
DRAWN BY:
Aditya Goturu
A4
SCALE:2:1
SHEET 4 OF 5

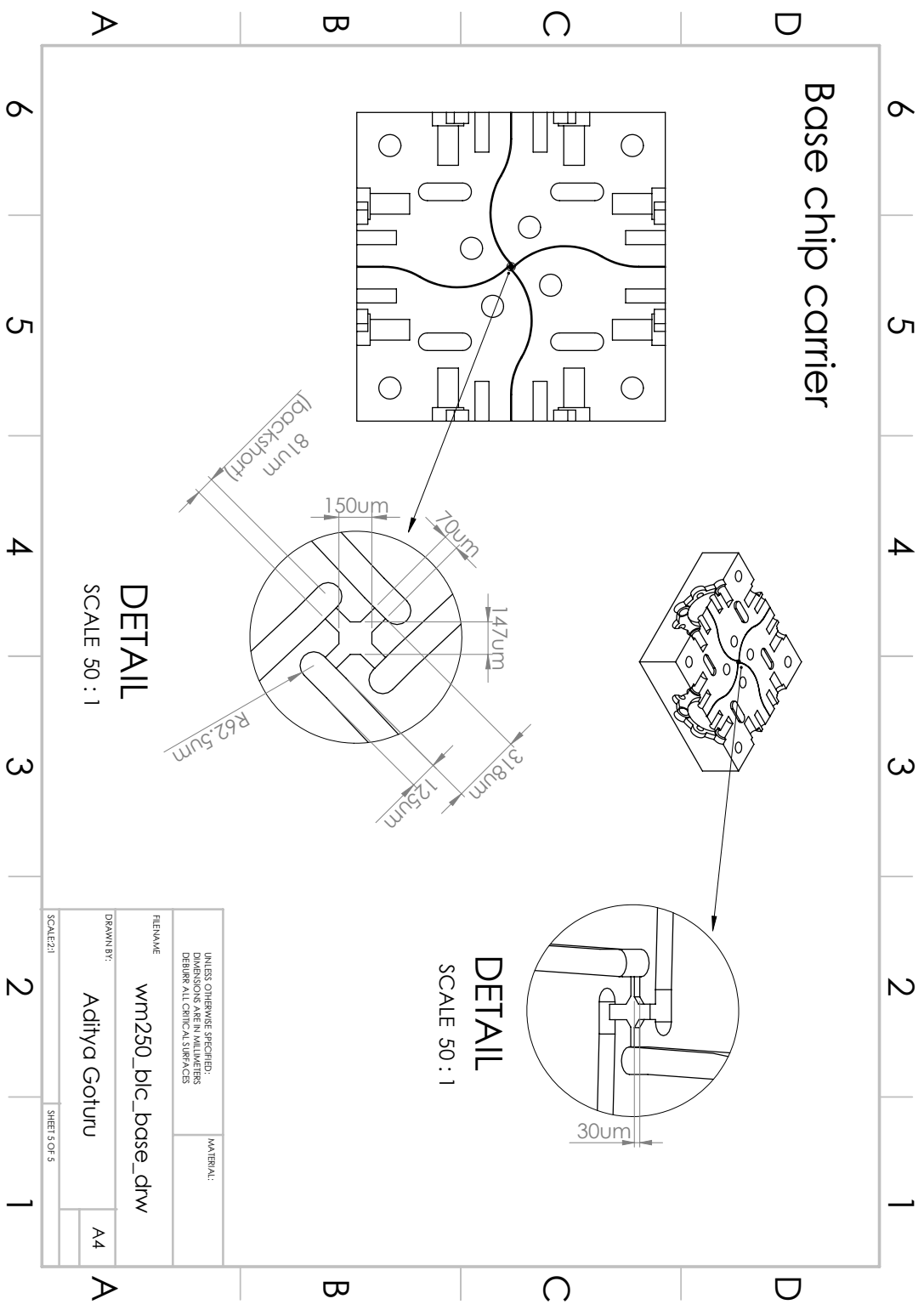
Base chip carrier
DETAIL
SCALE 50 : 1
DETAIL
SCALE 50 : 1
81um (backshort)
150um
70um
147um
R62.5um
125um
318um
30um
UNLESS OTHERWISE SPECIFIED:
DIMENSIONS ARE IN MILLIMETERS
DEBURR ALL CRITICAL SURFACES
MATERIAL:
FILENAME
wm250_blc_base_drw
DRAWN BY:
Aditya Goturu
A4
SCALE:2:1
SHEET 5 OF 5

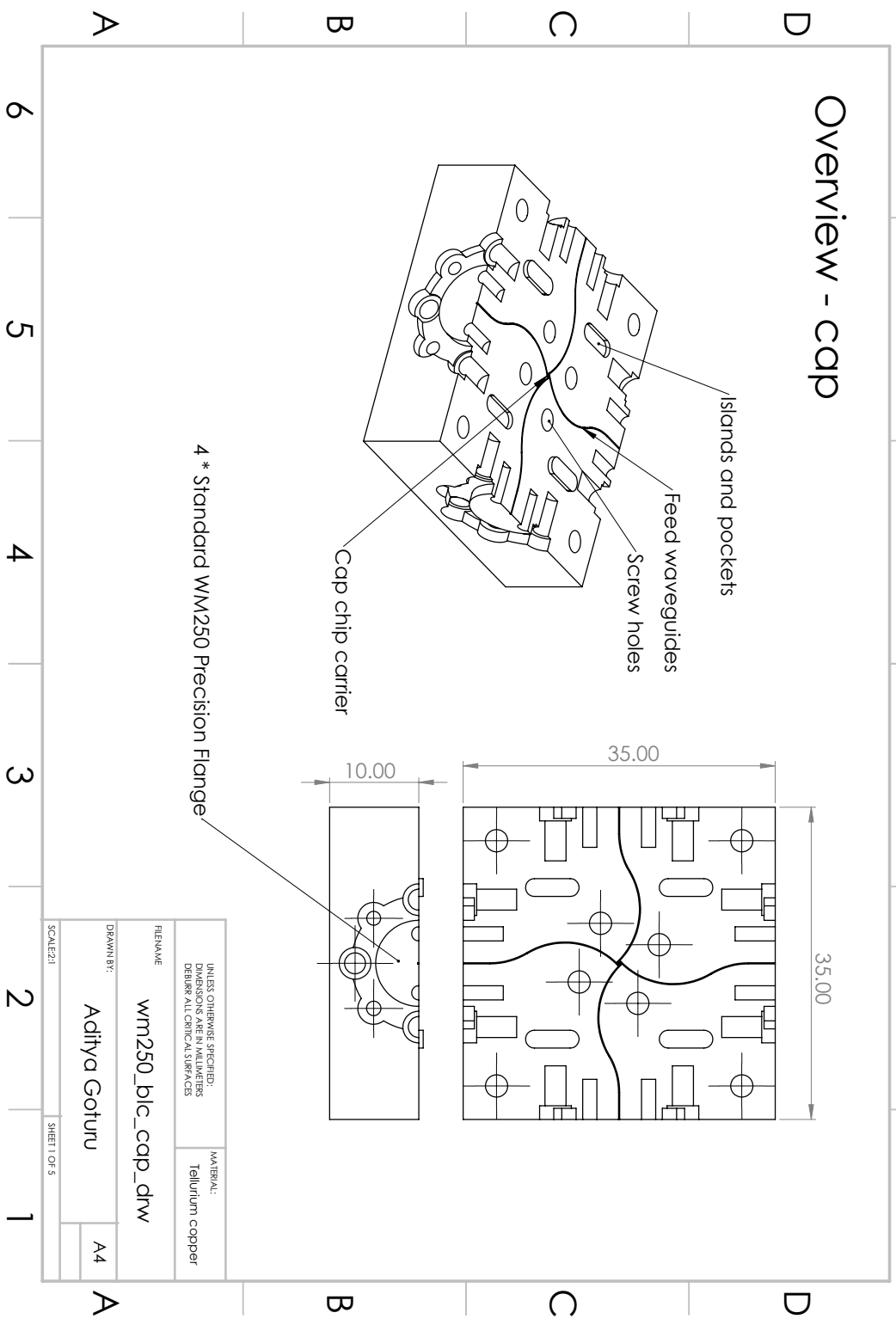
Overview - cap
Islands and pockets
Feed waveguides
Screw holes
Cap chip carrier
4 * Standard WM250 Precision Flange
35.00
35.00
10.00
UNLESS OTHERWISE SPECIFIED:
DIMENSIONS ARE IN MILLIMETERS
DEBURR ALL CRITICAL SURFACES
MATERIAL:
Tellurium copper
FILENAME
wm250_blc_cap_drw
DRAWN BY:
Aditya Goturu
A4
SCALE:2:1
SHEET 1 OF 5

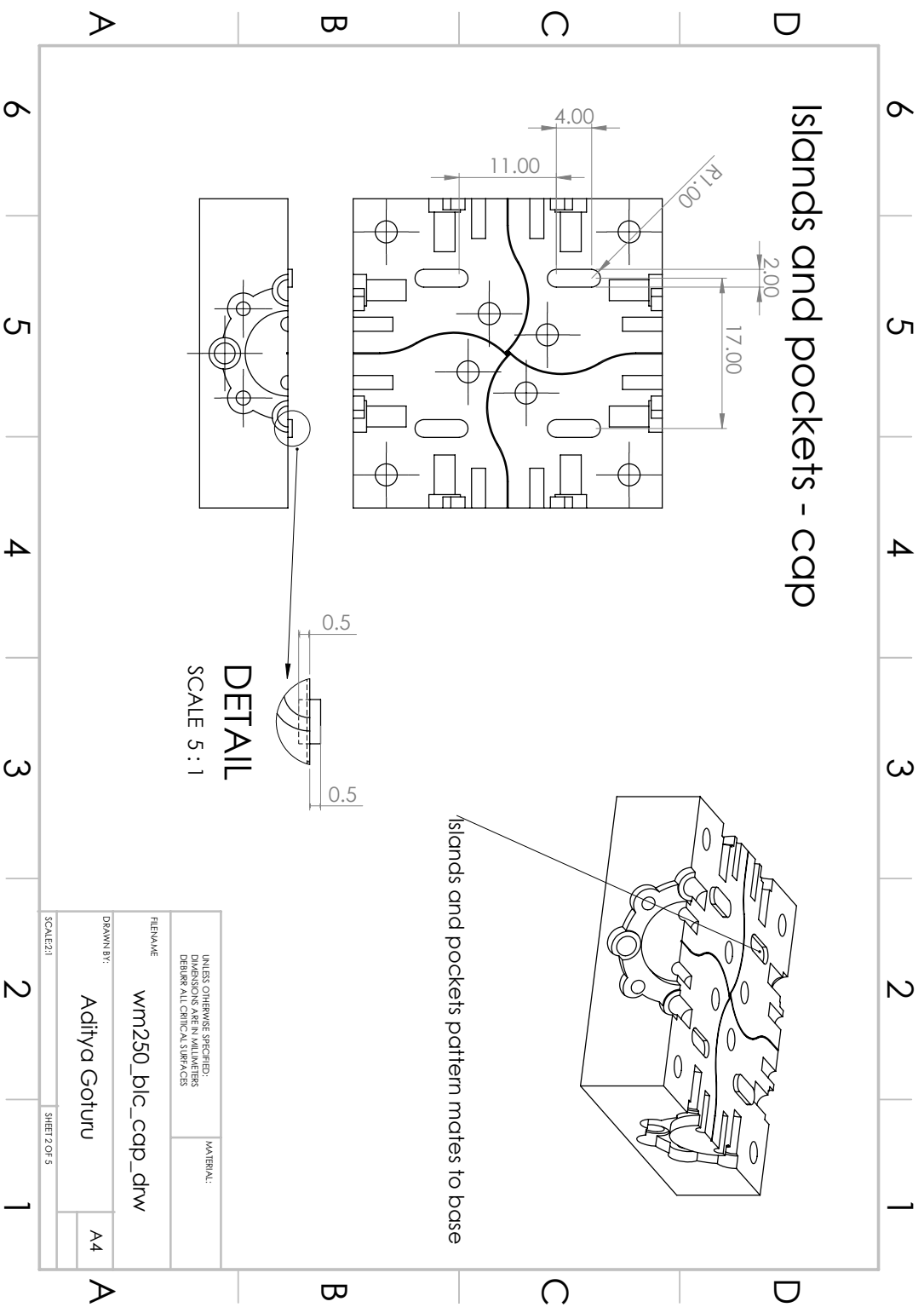
Islands and pockets - cap
4.00
11.00
R1.00
2.00
17.00
DETAIL
SCALE 5 : 1
0.5
0.5
Islands and pockets pattern mates to base
UNLESS OTHERWISE SPECIFIED:
DIMENSIONS ARE IN MILLIMETERS
DEBURR ALL CRITICAL SURFACES
MATERIAL:
FILENAME
wm250_blc_cap_drw
DRAWN BY:
Aditya Goturu
A4
SCALE:2:1
SHEET 2 OF 5

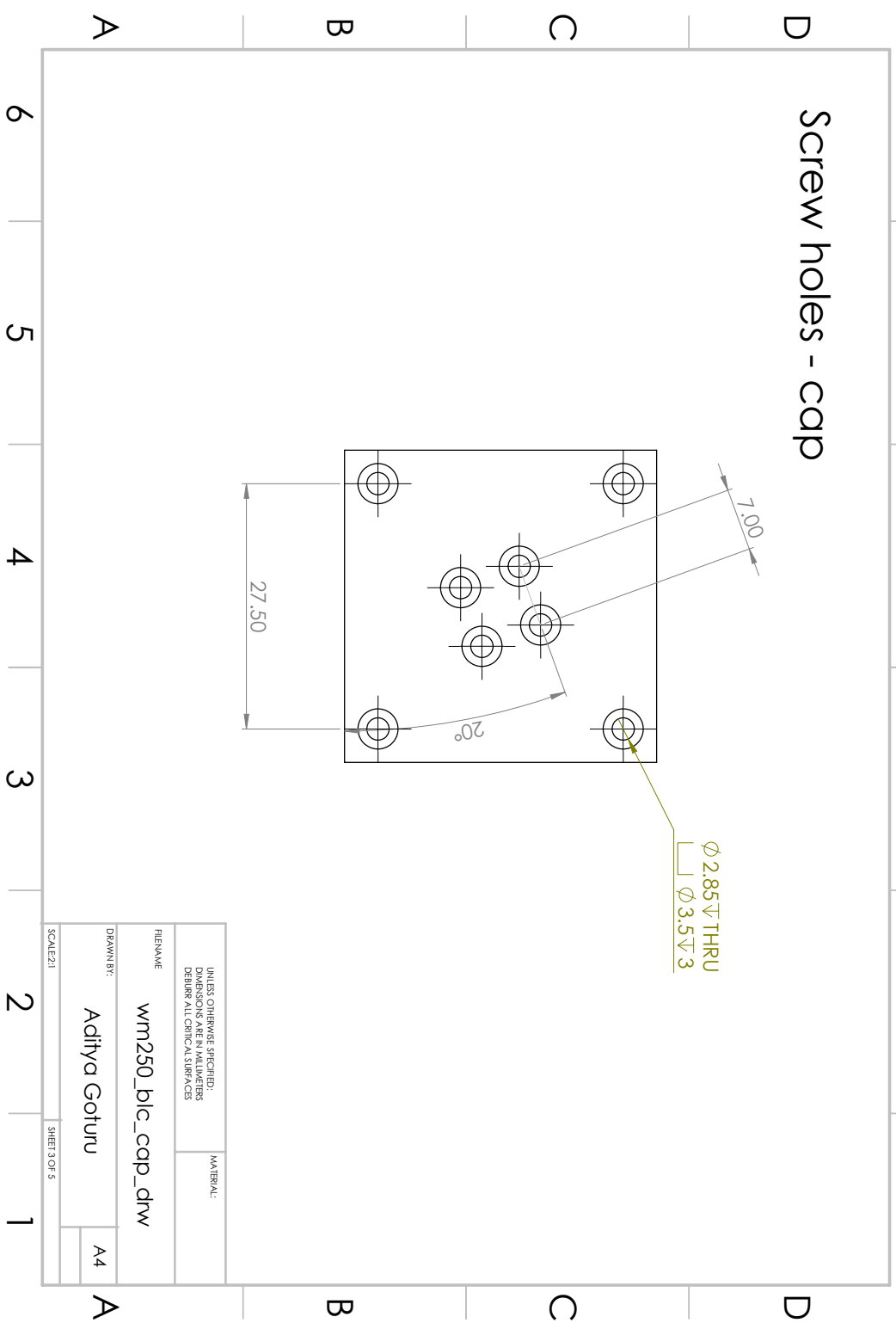
Screw holes - cap
7.00
27.50
20°
⌀2.85▽THRU
⌴ ⌀3.5▽3
UNLESS OTHERWISE SPECIFIED:
DIMENSIONS ARE IN MILLIMETERS
DEBURR ALL CRITICAL SURFACES
MATERIAL:
FILENAME
wm250_blc_cap_drw
DRAWN BY:
Aditya Goturu
A4
SCALE:2:1
SHEET 3 OF 5

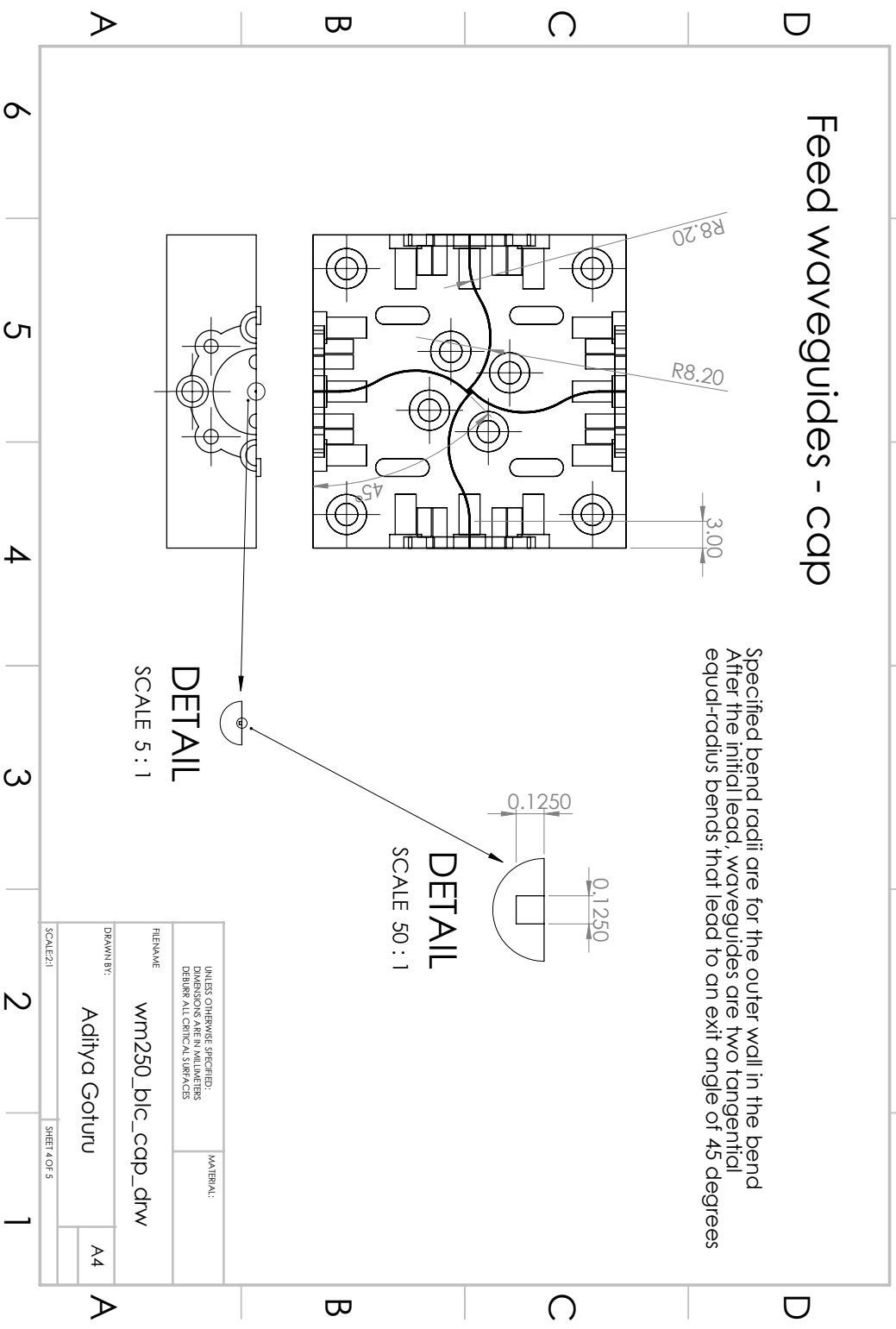
Feed waveguides - cap
R8.20
R8.20
45
3.00
Specified bend radii are for the outer wall in the bend
After the initial lead, waveguides are two tangential
equal-radius bends that lead to an exit angle of 45 degrees
DETAIL
SCALE 5 : 1
DETAIL
SCALE 50 : 1
0.1250
0.1250
UNLESS OTHERWISE SPECIFIED:
DIMENSIONS ARE IN MILLIMETERS
DEBURR ALL CRITICAL SURFACES
MATERIAL:
FILENAME
wm250_blc_cap_drw
DRAWN BY:
Aditya Goturu
A4
SCALE:2:1
SHEET 4 OF 5

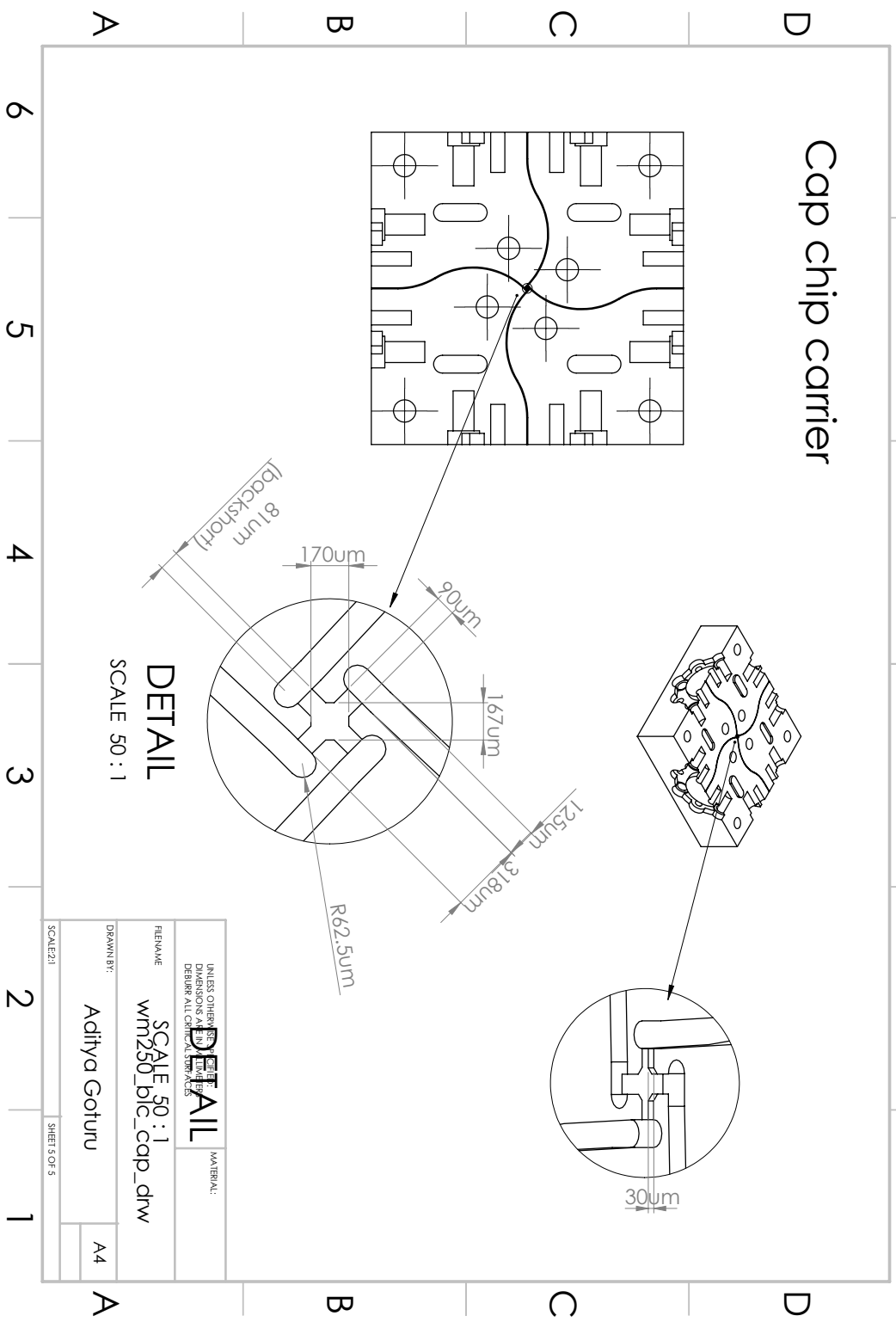
Cap chip carrier
DETAIL
SCALE 50 : 1
170um
90um
167um
125um
318um
R62.5um
81um
(backshort)
30um
DETAIL
SCALE 50 : 1
wm250_blc_cap_drw
Aditya Goturu
A4
SHEET 5 OF 5
SCALE:2:1

B

Appendix: Branch line coupler membrane drawings

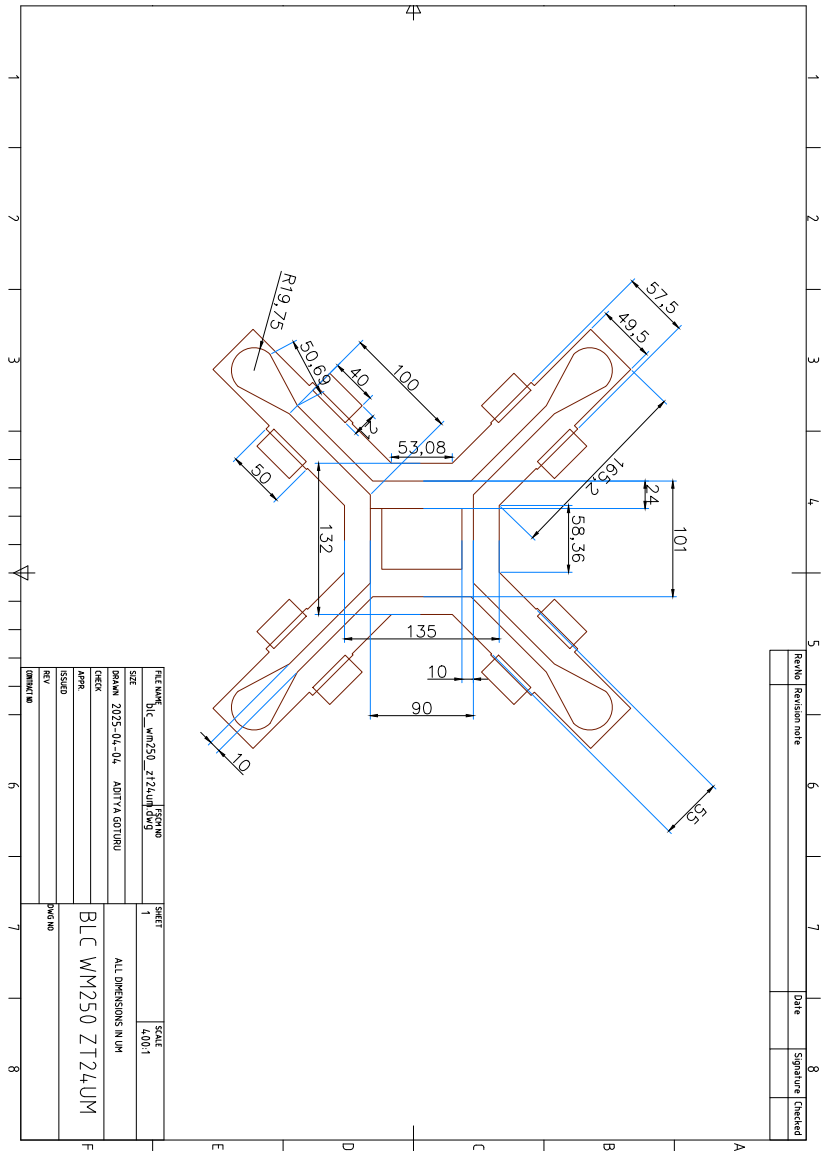

DEPARTMENT OF MICROTECHNOLOGY AND NANOSCIENCE
CHALMERS UNIVERSITY OF TECHNOLOGY
Gothenburg, Sweden
www.chalmers.se

CHALMERS
UNIVERSITY OF TECHNOLOGY